Faculdade de Engenharia da Universidade do Porto

Hellinger-Reissner variational principle in elastostatics

Monika Středulová

Master in Computational Mechanics

Supervisor: doc. Ing. Jan Eliáš, Ph.D.

Second Supervisor: Prof. Dr. José Manuel de Almeida César de Sá

July 22, 2021

Hellinger-Reissner variational principle in elastostatics

Monika Středulová

Master in Computational Mechanics

July 22, 2021

Abstract

The thesis describes the theoretical framework of Finite Element Method implementation based on variational principles and, subsequently, analyzes and compares results of two formulations based on different variational principles.

Fisrt, the governing equations of linear elastostatics are introduced, based on which the Minimum potential energy principle is described, followed by the Hellinger-Reissner variational principle.

The subsequent chapter derives the Finite Element Method in the context of other approximation methods and proceeds to formulate the stepping stones of the method, such as the discretization process and the definition of shape functions. Two elements are defined, the Q4 element based on the irreducible formulation and the Pian-Sumihara element, based on the Hellinger-Reissner mixed-field variational principle. Possible disadvantages of some Finite Element Method formulations are discussed with emphasis to the previously described elements.

Finally, Finite Element Method implementation requirements are described and possible methods to validate implementations are shown.

In the second part of the thesis the algorithm of the Finite Element Method implemented as a part of the thesis is discussed, followed by validation of the model in a form of a patch test and comparion of results to data in literature.

Subsequently, the two elements (Q4 and Pian-Sumihara) are tested in various situations and their response and differences are observed. Namely, the elements are tested in response to distortion, pure bending behaviour, combined shear and bending, and near incompressible material model combined with different types of element distortion. Benchmark cases found in literature are used and comparison to other elements results for the same cases is drawn where possible.

The element based on two field variational principle shows better results in all the examples, with significant differences between the two elements. The Pian-Sumihara element shows better behavior in bending as well as better response to the element distortion. In bending dominated situation coupled with shear the Q4 element produces highly underestimated results while the Pian-Sumihara element deliveres results of the same quality as other advanced methods which were tested on the same problem.

Keywords

Finite Element Method; Linear Elastostatics, Variational Principles, Principle of Minimum Potential Energy, Virtual Displacements, Hellinger-Reissner Variational Principle, Bilinear Quadrilateral Element, Pian-Sumihara Element

Acknowledgments

I would like to express my immense gratitude to both suppervisors of the thesis, doc. Ing. Jan Eliáš, Ph.D. and Prof. Dr. José Manuel de Almeida César de Sá. The amount of time you were willing to spend with me and the patience with which you shared your knowledge even from different corners of the world (even despite occasional technical difficulties) amazes me. I am grateful for the opportunity to develop this thesis under your supervision.

I would like to thank all the professors I have had the pleasure to meet in classes during the course of my studies at FEUP. You introduced me to new concepts, helped me see the field in greater context and always went out of your way to help, encourage and support us. I would like to specifically mention Prof. Marco Parente who I met in many courses, who has always found time to discuss any topic or fix software issues during the development of the thesis as well as during and between classes.

Thank you, my partners in crime for making me feel at home in a class almost full of brazilians and especially to Cindy Almeida. Your friendship throughout our studies means a lot to me. Thank you for reading any drafts, giving valuable comments, encouraging me and patiently discussing anything which was on my mind.

Thank you, Ing. Josef Květoň, Ph.D., for not hesitating in helping me.

Last but definitely not least, my gratitude goes to my family and wife. I would not be able to study this immensely interesting field if it were not for your ever lasting support and patience. Thank you from the bottom of my heart.

Monika Středulová

"Essentially, all models are wrong,
but some are useful."

George Box

Contents

List of Figures

List of Tables

List of Symbols

$\approx$	equals approximately
$^\circ$	degrees
^{e}	value in a local coordinate system
^{u}	primary (master) field to a secondary (slave) field
^{T}	transpose of a matrix or vector
a	distortion parameter
b	width of a beam
f	known function of a general problem
h	size of an element, depth of a beam
n_u, n_α	number f degrees of freedom associated to displacements, stresses
p	polynomial order
r	prescribed values of boundary conditions in general problem
t	thickness of a structure
u	unknown function of a general problem
x	position in a domain
A	linear differential operator
B	linear differential operator of boundary conditions
C_0	functions are connected at point
E	Young's modulus of elasticity
HR	Hellinger-Reissner functional
$\mathrm{HR}_{\mathrm{int}}$	internal potential energy of the Hellinger-Reissner functional
$\mathrm{HR}_{\mathrm{ext}}$	external potential energy of the Hellinger-Reissner functional
N	shape function
R	residual
$S_{\hat{t}}$	surface / edge where traction is applied
$S_{\hat{u}}$	surface / edge where displacement is prescribed
S	$S_{\hat{t}} \cup S_{\hat{u}}$
V	volume
W	weight function
$\mathbf{a}$	vector of unknown parameters
$\mathbf{b}$	body force
$\mathbf{f}$	load vector
$\hat{\mathbf{t}}$	traction
$\mathbf{u}$	displacement field, vector of displacements
$\hat{\mathbf{u}}$	vector of prescribed displacements (chapter 2), approximated solution (chapter 3 and further)

$\mathbf{B}$	matrix associating shape functions derivatives
$\mathbf{C}$	constitutive matrix in two dimensions
$\mathbf{D}$	matrix operator
$\mathbf{E}$	constitutive matrix
$\mathbf{G}$	transformation matrix of stress field
$\mathbf{H}$	matrix associating shape functions
$\mathbf{J}$	Jacobian matrix
$\mathbf{K}$	stiffness matrix
$\mathbf{P}_n$	projection matrix

α	angle of rotation
δ	first variation
ζ	third natural coordinate
η	second natural coordinate
λ_i	arbitrary function
λ	Lamé parameter
μ	shear modulus
ν	Poisson's coefficient
ξ	first natural coordinate
τ	shear stress
ϕ_i	known function which is equal to zero where boundary conditions are prescribed
ψ	known function which satisfies boundary conditions
Γ	boundary to the general problem where boundary conditions are defined
Π	potential energy
Π_{int}	internal potential energy
Π_{ext}	external potential energy
Ω	domain of a known function
$\boldsymbol{\alpha}$	vector of unknown stress parameters
$\boldsymbol{\varepsilon}$	strain field
$\boldsymbol{\sigma}$	stress field
$\boldsymbol{\tau}$	matrix of unknown stress parameters

Abreviations

2D	two dimensional
3D	three dimensional
CPU	central processing unit
DOF(s)	degree(s) of freedom
FEM	Finite Element Method
GP	Gauss point
PS	Pian-Sumihara element
Q4	bilinear isoparametric quadrilateral element
TC	test case

Chapter 1

Introduction

The Finite Element Method is a highly popular tool of today for solving differential equations. As such, it can be encountered in number of commercial softwares where it is applied on various problems, e. g. mechanical behavior of fluids or solids. In meachanics of solids, its use spans from the design of large civil engineering structures to smaller components in mechanical engineering. The method is particularly popular, among other reasons, for its relatively easy software implementation and the possibility of it's application to any domain shape. In mechanics of solids, any domain translates to differently shaped structures, allowing variablity of the structures to which the method may be applied.

The method is used as an approximation to mathematical models, which would be otherwise unsolvable or solvable only with immense difficulties. Generally, to take advantage of any mathematical model, it is essential to understand the assumptions which were made upon it's formulation.

The thesis aims to describe both of these parts of design of solid structures and components, the model and the method which is commonly used to solve it.

The first part of the thesis will describe the basic model of solid materials response to loading, that is the governing equations of linear elastostatics in three dimensions. Possible simplification to two dimensions will be also discussed. The equations present a boundary valued problem in strong form.

Naturally, alternative but equivalent forms of the governing equations also exist. The basis for the alternatives, also called weak forms, of the equations are basic physical principles. In the thesis the derivation of these principles, namely the Minimum potential energy principle, the principle of virtual work and an alternative mixed principle, from the strong formulation of the model of linear elastostatics will be described.

The following part will describe the Finite Element method to details. It will be first shortly discussed in a context of other approximation methods, only to proceed to the essential step of discretization and the formulation of the shape functions, which create the finite elements based on which the method received its name and which are the cornerstone of the method. Other steps to allow software implementation of the method will

be discussed, followed by definition of two elements for idelized two-dimensional problems of plane stress and plane strain with emphasis on the software implementation.

One of the most popular 2-D elements is the bilinear quadrilateral. The element approximates locally an unknown field and may be used for irreducible or mixed formulations.

The element is popular even in commercial software, however it is unable to obtain converging results for certain class of problems. In bending dominated situations, the shape of the element is not able to capture the deformation which results in occurence of spurious shear stresses, and subsequently, in a stiffer behavior of the element and underestimated displacements. Also in case of nearly incompressible material for which the Poisson's coefficient $\nu \to 0.5$, the element is not able to deform in a way which would allow to preserve the volume, resulting as well in a stiffer behavior.

Underestimating the deflection of a structure to loading is naturally undesirable in the design process and so the existence of such cases has been studied in the literature, resulting in development and possible remedies.

The goal of the thesis, apart from describing both the model and the method of solving the problem, is the implementation of an element based on the mixed-field variational principle, which approximates two fields instead of one field as in case of the irreducible formulation.

The second element which will be described is a quadrilateral element based on a mixed a principle, as developed by Pian and Sumihara in [5]. The element uses parameters to approximate two fields, displacements and stresses independently. It is an alternative element to overcome the issues of the displacement-based Q4 element.

To allow for a comparison between the two elements, finite element method algorithm will be developed as part of the thesis, with both elements implemented. To validate the implementation, a patch test will be performed and the elements will be applied to problems to simple problems from literature. Following the validation, the algorithm will be used to solve a series of problems involving shear and volumetric locking to observe differences between the two elements and their response to different types of loading and/or distortion.

Chapter 2

Linear elastostatics

2.1 Governing equations / strong formulation

Finite element method (FEM) around which the thesis revolves is only one possible way of (approximately) solving the governing equations of linear elasticity. Before formulating the method, it is first necessary to properly introduce the problem to which a solution is sought. Unless explicitly stated otherwise, the equations are taken from Applied mechanics of solids by Bower [7].

In mechanics of solids, a typical problem may be described in a following manner: a body positioned in a certain way undergoes a deformation as a result of internal and/or external loading and/or prescribed displacements. The amount of deformation which is induced and consequently the stress which occurs in the body as a result is of interest and serves as a basis for design or further research.

When a body is subjected to deformation, the process is commonly mathematicaly described in any point of the body (in the volume V of the body) by a displacement vector $\mathbf{u}$, strain tensor $\boldsymbol{\varepsilon}$ and stress tensor $\boldsymbol{\sigma}$ (three dimensional form of the vector and tensors is showed in Figure 2.1). Internal load is defined by vector $\mathbf{b}$ in the volume V of the body, loading acting on the surface $S_{\hat{t}}$ is defined by traction vector $\hat{\mathbf{t}}$ and displacement is prescribed by a vector $\hat{\mathbf{u}}$ on a surface $S_{\hat{u}}$.

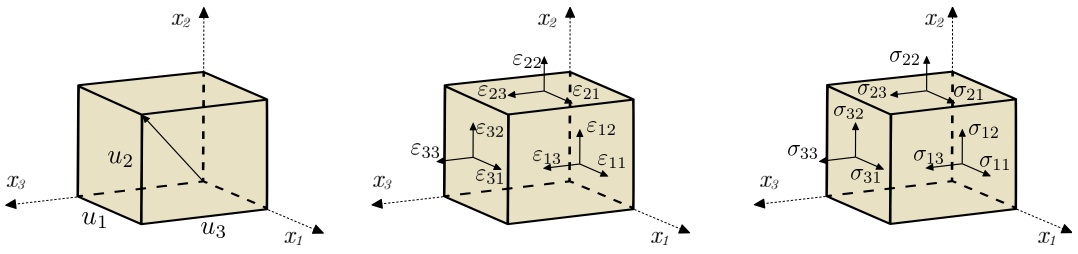

(a) Displacement vector $\mathbf{u}$. (b) Strain tensor $\boldsymbol{\varepsilon}$. (c) Stress tensor $\boldsymbol{\sigma}$.

Figure 2.1: Description of state at a point in three-dimensional linear elasticity.

Relationships between these variables may be of different forms, for example partial differential equations. However, they might be simplified by limiting the scope of the equations to account only for certain type of material behavior or time dependency of loading. By such simplification, linear elasticity is defined as a model describing very small and reversible deformation of a body, which does not depend on history of loading nor on the rate of loading. Furthermore, it also assumes linear dependency between stress and strain, which may or may not be the same in each direction (isotropic material, orthotropic and anisotropic material respectively). In addition, only small deformations, displacements and rotations are assumed.

By preserving the above written and considering equations defining relationships between variables to be valid in each point of the volume V or surface S, the so called *strong formulation* is defined. It may be conveniently described by Tonti diagram [8] (Figure 2.2) where relationships between variables are visualized along with the simplified equations.

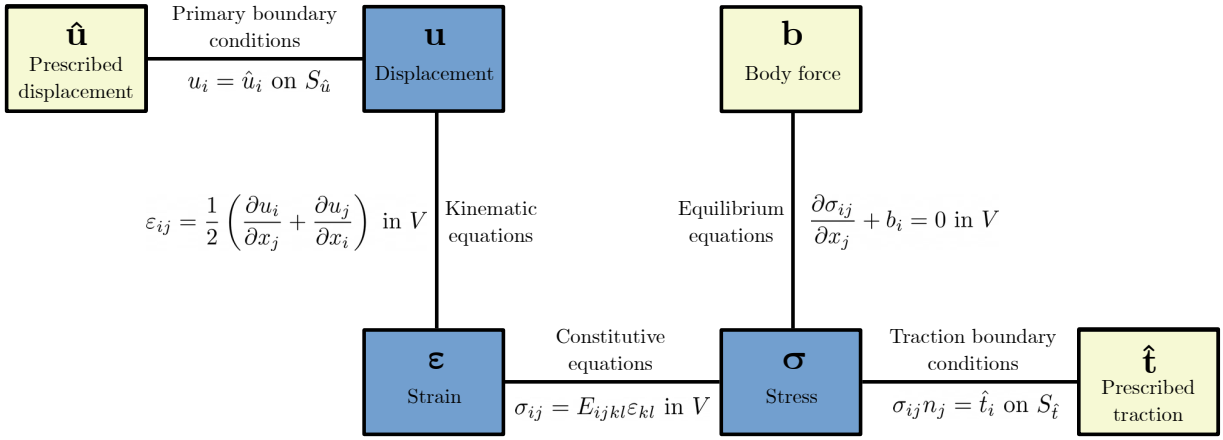

Figure 2.2: Strong formulation of linear elasticity described by Tonti diagram.

In the diagram, each rectangle represents a variable, with the yellow rectangle symbolizing entry data field and blue rectangle symbolizing unknown fields. The formulation is static, so it is also called a boundary value problem. Each link of the diagram is completed with the name of the equation and the equation itself in a component notation. The same equations may be found in Table 2.1 along with their matrix notation, which is often used for its conveniency in computer implementation.

			component notation	matrix notation
Kinematic equations	$\mathbf{u}$ - $\boldsymbol{\varepsilon}$	in V	$\varepsilon_{ij} = \frac{1}{2}\left(\frac{\partial u_i}{\partial x_j} + \frac{\partial u_j}{\partial x_i}\right)$	$\boldsymbol{\varepsilon} = \mathbf{D}\mathbf{u}$
Constitutive equations	$\boldsymbol{\varepsilon}$ - $\boldsymbol{\sigma}$	in V	$\sigma_{ij} = E_{ijkl}\varepsilon_{kl}$	$\boldsymbol{\sigma} = \mathbf{E}\boldsymbol{\varepsilon}$
Equilibrium equations	$\boldsymbol{\sigma}$ - $\mathbf{b}$	in V	$\frac{\partial \sigma_{ij}}{\partial x_j} + b_i = 0$	$\mathbf{D}^T\boldsymbol{\sigma} + \mathbf{b} = 0$
Displacement boundary conditions	$\hat{\mathbf{u}}$ - $\mathbf{u}$	on $S_{\hat{u}}$	$u_i = \hat{u}_i$	$\hat{\mathbf{u}} = \mathbf{u}$
Traction boundary conditions	$\boldsymbol{\sigma}$ - $\hat{\mathbf{t}}$	on $S_{\hat{t}}$	$\sigma_{ij} n_j = \hat{t}_i$	$\mathbf{P}_n\boldsymbol{\sigma} = \hat{\mathbf{t}}$

Table 2.1: Governing equations of linear elasticity.

Solution to elastostatic problem is to find displacement $\mathbf{u}$, strain $\boldsymbol{\varepsilon}$ and stress $\boldsymbol{\sigma}$ fields (see Tonti diagram in Figure 2.2) such that the boundary conditions and the governing equations are satisfied.

In three dimensions, displacement $\mathbf{u}$ is commonly represented by a vector $\mathbf{u} = \{\, u_1 \;\; u_2 \;\; u_3 \,\}^T$ (Figure 2.1a). Strain tensor $\boldsymbol{\varepsilon}$ (Figure 2.1b) may be casted to a vector containing only independent components as $\boldsymbol{\varepsilon} = \{\, \varepsilon_{11} \;\; \varepsilon_{22} \;\; \varepsilon_{33} \;\; 2\varepsilon_{23} \;\; 2\varepsilon_{13} \;\; 2\varepsilon_{12} \}^T$, because $\varepsilon_{ij} = \varepsilon_{ji}$. Relationship between displacements and strains is commonly referred to as the *kinematic equations*, where strain (the amount of deformation) is given by the symmetric gradient of displacement. In matrix notation, the gradient is represented by a matrix operator $\mathbf{D}$ as in the following equations.

$$\boldsymbol{\varepsilon} = \mathbf{D}\mathbf{u}$$

$$\begin{Bmatrix} \varepsilon_{11} \\ \varepsilon_{22} \\ \varepsilon_{33} \\ 2\varepsilon_{23} \\ 2\varepsilon_{13} \\ 2\varepsilon_{12} \end{Bmatrix} = \begin{bmatrix} \frac{\partial}{\partial x_1} & 0 & 0 \\ 0 & \frac{\partial}{\partial x_2} & 0 \\ 0 & 0 & \frac{\partial}{\partial x_3} \\ 0 & \frac{\partial}{\partial x_3} & \frac{\partial}{\partial x_2} \\ \frac{\partial}{\partial x_3} & 0 & \frac{\partial}{\partial x_1} \\ \frac{\partial}{\partial x_2} & \frac{\partial}{\partial x_1} & 0 \end{bmatrix} \begin{Bmatrix} u_1 \\ u_2 \\ u_3 \end{Bmatrix} \tag{2.1}$$

To ensure that the strains are integrable and it is hence possible to obtain displacements from the tensor, so called *compatibility equations* have to be satisfied. In component notation, the equation is following:

$$\frac{\partial^2 \varepsilon_{ij}}{\partial x_k \partial x_l} + \frac{\partial^2 \varepsilon_{kl}}{\partial x_i \partial x_j} - \frac{\partial^2 \varepsilon_{il}}{\partial x_j \partial x_k} - \frac{\partial^2 \varepsilon_{jk}}{\partial x_i \partial x_l} = 0 \tag{2.2}$$

Given a continuous body, satisfaction of these conditions means that there is a unique solution to the integration. In case of non-continuous bodies, the solution may not be unique.

Similarly to the strain tensor, stress tensor (Figure 2.1c) may also be cast to a vector as $\boldsymbol{\sigma} = \{ \sigma_{11} \;\; \sigma_{22} \;\; \sigma_{33} \;\; \sigma_{23} \;\; \sigma_{13} \;\; \sigma_{12} \}^T$. The two are linked via *constitutive equations*. Linear proportionality between stress and strain is given by the material matrix $\mathbf{E}$, also often denoted by $\mathbf{C}$ in literature. It contains parameters of the body's material, essentialy defining the body's response to a given strain. The matrix $\mathbf{E}$, describing Hooke's law, may be simplified due to its symmetry to an invertible [9] 6 by 6 matrix (Equation 2.4). For isotropic material the matrix depends two independent elastic constants: modulus of elasticity E and Poisson's coefficient ν. The constitutive equation has the following form:

$$\boldsymbol{\sigma} = \mathbf{E}\boldsymbol{\varepsilon}$$

$$\begin{Bmatrix} \sigma_{11} \\ \sigma_{22} \\ \sigma_{33} \\ \sigma_{23} \\ \sigma_{13} \\ \sigma_{12} \end{Bmatrix} = \frac{E}{(1+\nu)(1-2\nu)} \begin{bmatrix} 1-\nu & \nu & \nu & 0 & 0 & 0 \\ \nu & 1-\nu & \nu & 0 & 0 & 0 \\ \nu & \nu & 1-\nu & 0 & 0 & 0 \\ 0 & 0 & 0 & \frac{1-2\nu}{2} & 0 & 0 \\ 0 & 0 & 0 & 0 & \frac{1-2\nu}{2} & 0 \\ 0 & 0 & 0 & 0 & 0 & \frac{1-2\nu}{2} \end{bmatrix} \begin{Bmatrix} \varepsilon_{11} \\ \varepsilon_{22} \\ \varepsilon_{33} \\ 2\varepsilon_{23} \\ 2\varepsilon_{13} \\ 2\varepsilon_{12} \end{Bmatrix} \tag{2.3}$$

$$\boldsymbol{\varepsilon} = \mathbf{E}^{-1}\boldsymbol{\sigma} \tag{2.4}$$

Relationship between stress in the body $\boldsymbol{\sigma}$ to the body forces defined by the vector $\mathbf{b} = \{ b_1 \;\; b_2 \;\; b_3 \}^T$ is defined by the *equilibrium equations*, where matrix $\mathbf{D}^T$ is the transpose of the matrix operator of the kinematic equations (Eq. 2.1).

$$\mathbf{D}^T\boldsymbol{\sigma} + \mathbf{b} = 0$$

$$\begin{bmatrix} \frac{\partial}{\partial x_1} & 0 & 0 & 0 & \frac{\partial}{\partial x_3} & \frac{\partial}{\partial x_2} \\ 0 & \frac{\partial}{\partial x_2} & 0 & \frac{\partial}{\partial x_3} & 0 & \frac{\partial}{\partial x_1} \\ 0 & 0 & \frac{\partial}{\partial x_3} & \frac{\partial}{\partial x_2} & \frac{\partial}{\partial x_1} & 0 \end{bmatrix} \begin{Bmatrix} \sigma_{11} \\ \sigma_{22} \\ \sigma_{33} \\ \sigma_{23} \\ \sigma_{13} \\ \sigma_{12} \end{Bmatrix} + \begin{Bmatrix} b_1 \\ b_2 \\ b_3 \end{Bmatrix} = 0 \tag{2.5}$$

Displacement boundary condition simply states that, on a given surface $S_{\hat{u}}$, the resulting displacement $\mathbf{u}$ has to be equal to the prescribed displacement $\hat{\mathbf{u}}$. Stress field and prescribed traction are related by *traction boundary condition*. In component notation, n_j is an outward unit normal relating stress to the traction on a specified surface $S_{\hat{t}}$. In matrix notation, stress is represented by a vector of six independent components and traction is represented by $\hat{\mathbf{t}} = \{ \hat{t}_1 \;\; \hat{t}_2 \;\; \hat{t}_3 \}^T$. Relation between them is provided by the projection matrix $\mathbf{P}_n$.

$$\mathbf{P}_n\boldsymbol{\sigma} = \hat{\mathbf{t}}$$

$$\begin{bmatrix} n_1 & 0 & 0 & 0 & n_3 & n_2 \\ 0 & n_2 & 0 & n_3 & 0 & n_1 \\ 0 & 0 & n_3 & n_2 & n_1 & 0 \end{bmatrix} \begin{Bmatrix} \sigma_{11} \\ \sigma_{22} \\ \sigma_{33} \\ \sigma_{23} \\ \sigma_{13} \\ \sigma_{12} \end{Bmatrix} = \begin{bmatrix} \hat{t}_1 \\ \hat{t}_2 \\ \hat{t}_3 \end{bmatrix} \tag{2.6}$$

2.1.1 Plane stress and plane strain

Commonly, the three-dimensional description from the previous part may be further simplified. Typical examples of such simplification are plane stress, plane strain states or axisymmetrical idealization [1]. Only the first two are descibed in this section, since they will be later applied in case analysis. Axisymmetric idealization is described for example in [10].

For both plane stress and plane strain, the unknown displacements, strains and stresses are related to two dimensions, while variables related to the third dimension are either assumed to be equal to zero or made dependent. The displacement vector and the tensors then have the form as written below.

$$\begin{aligned} \mathbf{u} &= \{\, u_1, u_2 \}^T \\ \boldsymbol{\varepsilon} &= \{ \varepsilon_{11},\ \varepsilon_{22}, \varepsilon_{12}\ \}^T \\ \boldsymbol{\sigma} &= \{\, \sigma_{11}, \sigma_{22}, \sigma_{12}\ \}^T \end{aligned}$$

As the name suggests, in the case of plane stress all the stresses are parallel to one plane. It is often used to model thin plates loaded in the central plane of longest dimension of the plate. Strain in the third direction, ε_{33} is dependent on σ_{11} and σ_{22}, while $\varepsilon_{31} = \varepsilon_{32} = 0$. Displacement in the third direction is directly proportionate to the third coordinate. Components of the stress tensor related to the out-of-plane direction, in this case denoted by index $_3$, are equal to zero: $\sigma_{33} = \sigma_{13} = \sigma_{23} = 0$, while the other stresses are independent of the third coordinate. Figure 2.3 shows the non-zero components of plane stress states, while Eq. 2.7 shows the constitutive equation of plane stress.

$$\begin{Bmatrix} \sigma_{11} \\ \sigma_{22} \\ \sigma_{12} \end{Bmatrix} = \frac{E}{1-\nu^2} \begin{bmatrix} 1 & \nu & 0 \\ \nu & 1 & 0 \\ 0 & 0 & \frac{1-2\nu}{2} \end{bmatrix} \begin{Bmatrix} \varepsilon_{11} \\ \varepsilon_{22} \\ \varepsilon_{12} \end{Bmatrix} \tag{2.7}$$

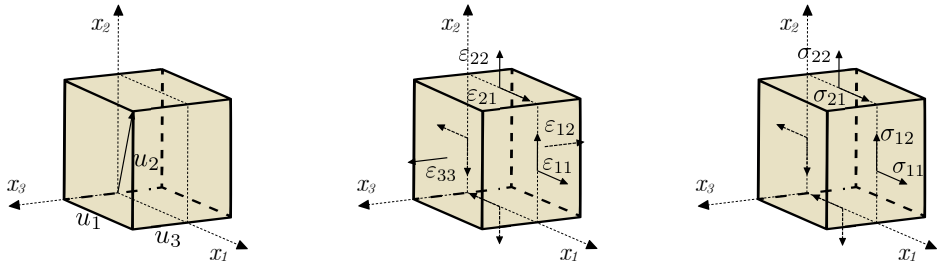

(a) Non-zero components of the displacement vector $\mathbf{u}$.

(b) Non-zero components of the strain tensor $\boldsymbol{\varepsilon}$.

(c) Non-zero components of the stress tensor $\boldsymbol{\sigma}$.

Figure 2.3: Plane stress.

In the case of plane strain, no displacement occurs in the third direction, implying $\varepsilon_{33} = \varepsilon_{13} = \varepsilon_{23} = 0$. However, to achieve this, the stress component of the third direction $\sigma_{33} \neq 0$ and is a dependent variable, while $\sigma_{13} = \sigma_{23} = 0$. The non-zero components are depicted in Figure 2.4. Equation 2.6 describes the constitutive relation of plane strain.

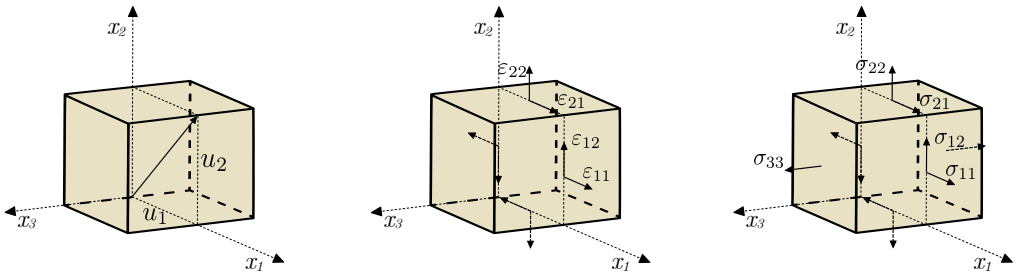

(a) Non-zero components of the displacement vector $\mathbf{u}$,

(b) non-zero components of the strain tensor $\boldsymbol{\varepsilon}$,

(c) non-zero components of the tress tensor $\boldsymbol{\sigma}$.

Figure 2.4: Plane strain.

$$\begin{Bmatrix} \sigma_{11} \\ \sigma_{22} \\ \sigma_{12} \end{Bmatrix} = \frac{E}{(1+\nu)(1-2\nu)} \begin{bmatrix} 1-\nu & \nu & 0 \\ \nu & 1-\nu & 0 \\ 0 & 0 & \frac{1-2\nu}{2} \end{bmatrix} \begin{Bmatrix} \varepsilon_{11} \\ \varepsilon_{22} \\ \varepsilon_{12} \end{Bmatrix} \tag{2.8}$$

2.2 Weak form of the governing equations

In the formulation described in the previous section, the governing equations (Table 2.1) are satisfied at every point of the body. Unless a specific case is being solved, it is not possible to obtain analytical solution via the strong form of the equations [1].

One of the possible approaches to finding a solution to a more general problem is to relax some of the equations from Table 2.1 by transforming the strong links, represented by equations which are to be satisfied at each point, to weak links, which satisfy them in a weak, average sense.

The relaxation is performed by multiplying the equation by a function λ_i, whose value is arbitrary, except for the surface where essential boundary condition[1] is applied, where the value of the arbitrary function equals to zero [1]. The function may be interpreted in multiple ways which will be discussed later when applied to a particular formulation. The multiplied equation is then integrated over the domain where the equation is defined. The resulting weak form thus has the form of a functional and is also called integral form of a differential equation.

Example of a weak form of the equilibrium equation is given below.

strong form	**weak form**
$\frac{\partial \sigma_{ij}}{\partial x_j} + b_i = 0$	$\int_V \left(\frac{\partial \sigma_{ij}}{\partial x_j} + b_i \right) \lambda_i \, dV = 0$

Table 2.2: Strong and weak forms of the equilibrium equation.

By assigning an arbitrary value to the function λ_i, the equation is satisfied at every point and the weak form is equivalent to the strong form [11].

Multiple interpretations of the function λ_i are found in literature, as well as notation of the function. For example Tchonkova [12] writes about test function in the context of irreducible displacement model (section 2.2.1) and about the Lagrange multiplier in context of the mixed formulation (section 2.2.2). If displacement variation is used, the method is dubbed virtual displacements method [13].

Besides transforming strong links to weak links, it is necessary in the solving process to select one or more primary fields from the unknown fields (displacement, stress and strain fields, represented with blue background in Figure 2.2). The primary fields will be later varied and obtained first in the solving process, with the other, secondary, field(s) being derived from the primary field(s). If only one field serves as the primary field, the resulting formulation is also called irreducible, otherwise the term mixed formulation is used for a multiple primary fields formulation [1].

Multiple combinations of weak links and primary field(s) may be chosen to solve the governing equations, which may serve as a basis for a particular Finite Element method formulation, however, some have proven to be more advantageous in solving the governing equations than others for different types of structures [7].

[1] Essential boundary conditions are enforced via strong links.

One of the most widely used forms is the displacement-based formulation, where displacement is the only primary variable. It leads to a displacement-based Finite Element method technique, which is usually implemented in commercial FEM softwares, such as Abaqus [14]. The formulation will be described in the subsequent section 2.2.1. By weakening the equilibrium equation, the total potential energy variational principle may be derived, which will also be demonstrated in the section.

Subsequently, a mixed formulation with two primary fields will be presented in section 2.2.2 as a potential alternative to the irreducible displacement model, leading to the Hellinger-Reisner variational principle.

2.2.1 Displacement based formulation

As briefly mentioned in the previous paragraph, displacement based form is a one primary field, irreducible formulation. Strain and stress fields are related to the displacement field via strong links, which is reflected by a slight change in notation by adding upper index $^{\mathbf{u}}$: strain and stress fields are denoted by $\boldsymbol{\varepsilon}^u$ and $\boldsymbol{\sigma}^u$ respectively. Due to their dependency on the primary field they are also called secondary fields. Equilibrium equation and traction boundary condition are weakened via similar procedure to the one described previously. The Tonti diagram of the displacement irreducible model is shown below, complemented by a table summarazing the equations on the next page.

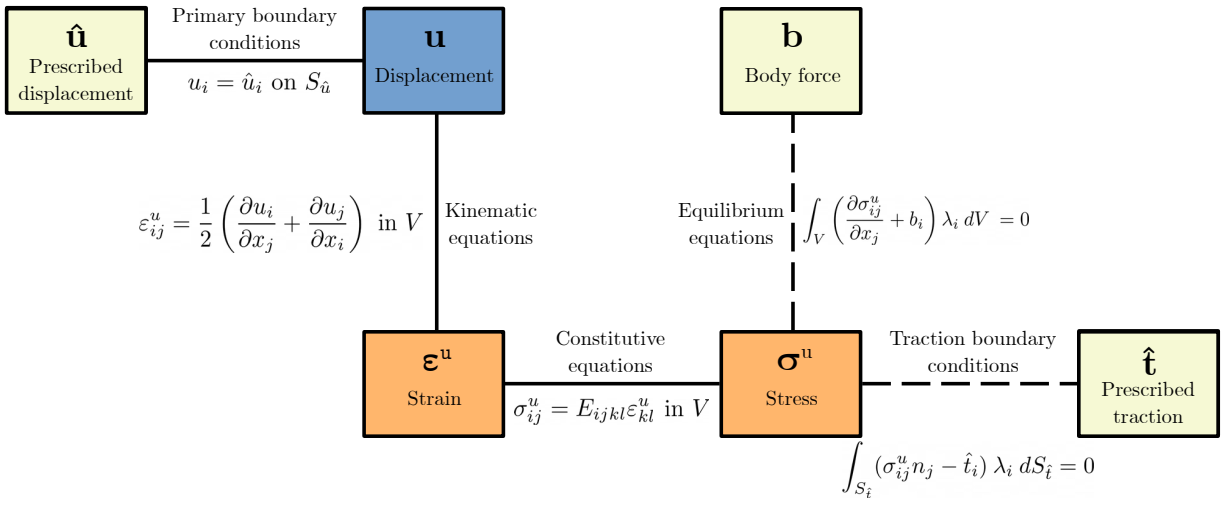

Figure 2.5: Displacement based formulation of linear elasticity as described by Tonti diagram.

In case of the present formulation, the arbitrary three-dimensional function λ_i (whose value is equal to zero where essential boundary condition is defined) may be interpreted as a variation of the displacement field, which translates the procedure to a virtual displacements method:

$$\lambda_i = \delta u_i = \{\delta u_1, \delta u_2, \delta u_3\}^T$$

			Type of link	Equation in component notation
Kinematic equations	$\mathbf{u}$ - $\boldsymbol{\varepsilon}^{\mathrm{u}}$	in V	strong	$\varepsilon_{ij}^u = \frac{1}{2}\left(\frac{\partial u_i}{\partial x_j} + \frac{\partial u_j}{\partial x_i}\right)$
Constitutive equations	$\boldsymbol{\varepsilon}^{\mathrm{u}}$ - $\boldsymbol{\sigma}^{\mathrm{u}}$	in V	strong	$\sigma_{ij}^u = E_{ijkl}\varepsilon_{kl}^u$
Equilibrium equations	$\boldsymbol{\sigma}^{\mathrm{u}}$ - $\mathbf{b}$	in V	weak	$\int_V \left(\frac{\partial \sigma_{ij}^u}{\partial x_j} + b_i\right) \delta u_i \, dV = 0$
Displacement boundary conditions	$\hat{\mathbf{u}}$ - $\mathbf{u}$	on $S_{\hat{u}}$	strong	$u_i = \hat{u}_i$
Traction boundary conditions	$\boldsymbol{\sigma}^{\mathrm{u}}$ - $\hat{\mathbf{t}}$	on $S_{\hat{t}}$	weak	$\int_{S_{\hat{t}}} (\sigma_{ij}^u n_j - \hat{t}_i)\, \delta u_i \, dS_{\hat{t}} = 0$

Table 2.3: Displacement based model of linear elasticity.

By weakening the equlibrium equation, an expression corresponding to the exact variation of the total potential energy of a system Π with respect to displacement is obtained $\Pi(\mathbf{u} + \delta\mathbf{u}) = \delta\Pi$, thus also justifiyng the interpretation of the function λ_i as a virtual displacement.

In mathematical sense, a stationary form of the functional is acquired by vanishing the first variation as:

$$\delta\Pi = 0 \tag{2.9}$$

In the present single field formulation, the only possible stationary form of the functional Π is extremal: minimum of the total potential energy functional. As such the Equation 2.9 is also known as the minimum of the total potential energy principle.

The procedure of obtaining the principle from the equations listed in Table 2.3 above is described in the following paragraph, based on the process shown in [9], where also a more detailed account of the procedure may be found.[2] The equation of total potential energy along with interpretation of its terms is given at the end.

The minimum potential energy principle from weak formulation In the first part of the process, the weak form of the equilibrium equation is used. To make orientation in the equations better, concatenated index notation is used for partial derivatives so

[2] The process is also often described inversely as the weak form of the governing equations may be derived from the minimum potential energy principle [11].

$\frac{\partial \sigma^u_{ij}}{\partial x_j} = \sigma^u_{ij,j}$. Additionaly, in the subsequent equations, surface S is the union of surfaces where boundary conditions are defined as $S = S_{\hat{t}} \cup S_{\hat{u}}$.

$$\int_V \left(\sigma^u_{ij,j} + b_i\right) \delta u_i \, dV = 0 \tag{2.10}$$

The first term of the equation may be altered in the following manner using the Gauss divergence theorem [18].

$$\int_V \sigma^u_{ij,j} \delta u_i \, dV = -\int_V \sigma^u_{ij} \delta u_{i,j} \, dV + \int_S \sigma^u_{ij} n_j \delta u_i \, dS \tag{2.11}$$

$$= -\int_V \sigma^u_{ij} \frac{1}{2}(\delta u_{i,j} + \delta u_{j,i}) \, dV + \int_S \sigma^u_{ij} n_j \delta u_i \, dS \tag{2.12}$$

$$= -\int_V \sigma^u_{ij} \delta \varepsilon^u_{ij} \, dV + \int_S \sigma^u_{ij} n_j \delta u_i \, dS \tag{2.13}$$

The Equation 2.13 may be deduced from Equation 2.12 because of the strong link between displacements and strains. In this step the strain field is essential substituted for the strong form of the kinematic equation.

Subsequently, it is possible to substitute the expression of Equation 2.13 into Equation 2.10, obtaining the expression:

$$-\int_V \sigma^u_{ij} \delta \varepsilon^u_{ij} \, dV + \int_S \sigma^u_{ij} n_j \delta u_i \, dS + \int_V b_i \delta u_i \, dV = 0 \tag{2.14}$$

The surface integral over the united boundary condition surfaces may be separated for each boundary condition type. The integral over $S_{\hat{u}}$ contains variation of displacement δu_i. By definition, the variation is equal to zero where kinematic boundary condition is applied, yielding the whole term equal to zero (Equation 2.15). Consequently, the equation may be altered to Equation 2.16.

$$\int_S \sigma^u_{ij} n_j \delta u_i \, dS = \int_{S_{\hat{u}}} \sigma^u_{ij} n_j \delta \hat{u}_i \, dS_{\hat{u}} + \int_{S_{\hat{t}}} \sigma^u_{ij} n_j \delta u_i \, dS_{\hat{t}} = \int_{S_{\hat{t}}} \sigma^u_{ij} n_j \delta u_i \, dS_{\hat{t}} \tag{2.15}$$

$$-\int_V \sigma^u_{ij} \delta \varepsilon^u_{ij} \, dV + \int_{S_{\hat{t}}} \sigma^u_{ij} n_j \delta u_i \, dS_{\hat{t}} + \int_V b_i \delta u_i \, dV = 0 \tag{2.16}$$

From the weak form of traction boundary condition an equivalent form of the traction surface integral may be obtained (Equation 2.17).

$$\int_{S_{\hat{t}}} (\sigma^u_{ij} n_j - \hat{t}_i) \, \delta u_i \, dS_{\hat{t}} = 0 \quad \longrightarrow \quad \int_{S_{\hat{t}}} \sigma^u_{ij} n_j \, \delta u_i \, dS_{\hat{t}} = \int_{S_{\hat{t}}} \hat{t}_i \delta u_i \, dS_{\hat{t}} \tag{2.17}$$

Substitution into the equation than conveniently introduces the traction vector $\hat{t}$ into the expression. Resulting equation obtained by the substitution for the surface integral is known as the weak form of the boundary value problem. The equivalency to the variation of the total potential energy of the system with respect to the displacement vector $\Pi(\mathbf{u}+\delta\mathbf{u}) = \delta\Pi = 0$ (Equation 2.18) is shown in the subsequent paragraph.

$$-\int_V \sigma_{ij}^u \delta\varepsilon_{ij}^u \, dV + \int_{S_{\hat{t}}} \hat{t}_i \delta u_i \, dS_{\hat{t}} + \int_V b_i \delta u_i \, dV = 0 \tag{2.18}$$

The minimum potential energy principle According to Washizu, the principle may be stated as follows: "Among all the admissible displacements u_i which satisfy the prescribed geometrical boundary conditions, the actual displacements make the total potential energy stationary." [9, p. 28]

The total potential energy of a system Π consists of two parts: the internal potential energy Π_{int} and the external potential energy Π_{ext}:

$$\Pi = \Pi_{\text{int}} - \Pi_{\text{ext}}$$

$$\Pi_{\text{int}} = \frac{1}{2}\int_V \sigma_{ij}^u \varepsilon_{ij}^u \, dV$$
$$\Pi_{\text{ext}} = \int_{S_{\hat{t}}} \hat{t}_i u_i \, dS_{\hat{t}} + \int_V b_i u_i \, dV$$

The internal potential energy is essentialy the sum of the strain energy density stored in the body $\mathrm{U} = \frac{1}{2}\sigma_{ij}^u \varepsilon_{ij}^u$. The external potential energy describes the energy density of the external forces, which are the traction $\hat{t}_i$ applied on the surface $S_{\hat{t}}$ and the body force b_i acting in the volume of the body V.

Both Π_{int} and Π_{ext} describe the work which is done by the respective forces, whether internal or external, by a potential of these forces. The combination of the two suggests that the resulting displacement field places the system in a state of static equilibrium.

It was previously mentioned, that the variation with respect to displacement field is called the virtual displacement method. Following the work interpretation of the potential energy given above, the equation 2.18 may be also explained in a wider context as a specific case of the principle of virtual work, the principle of virtual displacements. In this case, the virtual work is done by applied (real) forces on the virtual displacements, which are expressed in the mathematical formula as a variation of displacmenets δu_i.

Another one field variational principle often used is a total complementary energy principle, also called Castigliani's principle [9]. Analogically to the irreducible displacement-based model which was described in this section, Castigliani's principle is based on the stress field as a primary variable, with respect to which the total potential energy is varied and

base on which the strain field and displacement vector is obtained. The procedure is also called the principle of virtual forces, where virtual work is computed as the work done by virtual forces done real displacements, which is also specific example of the principle of virtual work. According to Washizu [9], the total potential energy principle and the total complementary energy principle are: "reciprocal and equivalent to each other as far as the small displacement theory of elasticity is concerned".

2.2.2 Hellinger-Reissner variational principle

The previous model has seen the variation of displacements as a means of obtaining the minimum of the total potential energy. As a possible extension to the procedure, the variation of another field may be added, leading to a two-field variational principle. From a mathematical point of view, the two field principle may be constructed by choosing any internal field, that is displacement, strain, or stresses. One of the more widely known and used is the Hellinger-Reissner variational principle, in which variation of stress and displacement field is done [15].

As in the previous cases, the principle is represented by Tonti's diagram [8] in Figure 2.6.

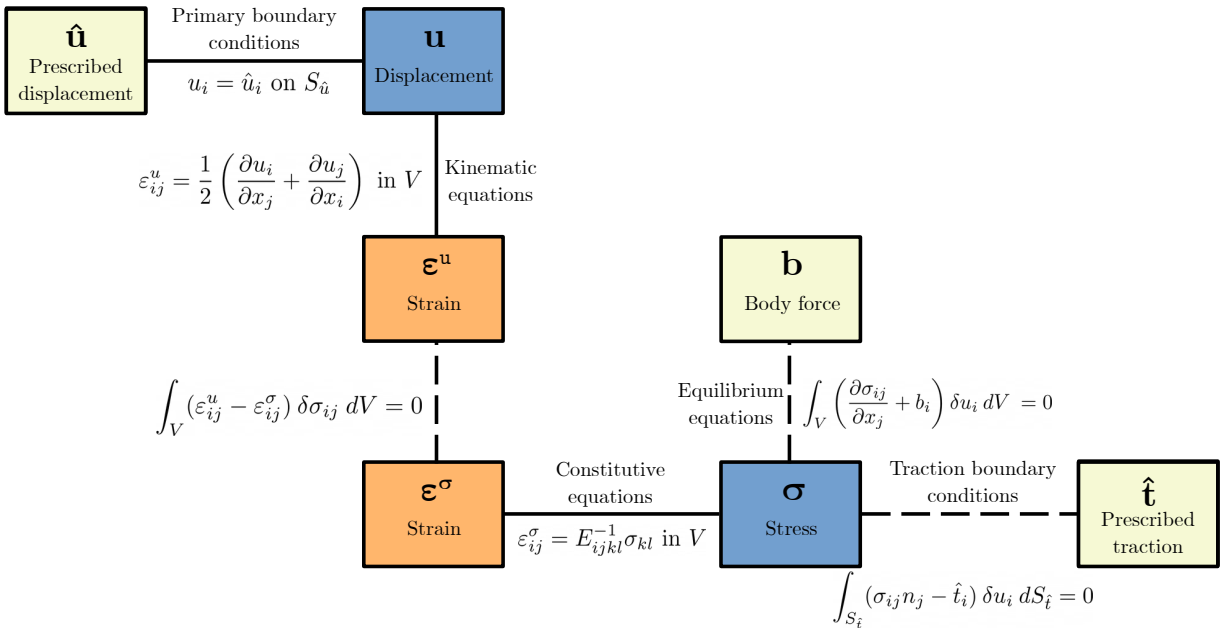

Figure 2.6: Tonti's diagram of the Hellinger-Reissner variational principle.

There are two primary fields: displacement and stress field. Two slave fields are present, following the notation outlined in the previous section, the strain field $\boldsymbol{\varepsilon}^{\mathrm{u}}$ is obtained via kinematic equation and the strain field $\boldsymbol{\varepsilon}^{\sigma}$ is obtained by inverting the constitutive law as in the context of linear elasticity, the material matrix $\mathbf{E}$ is invertible. Connection between the two strain fields is weak, created via the same method as in the previous cases. As in the irreducible displacement-based formulation, the equilibrium equation and the traction boundary condition remain in the weak form.

All of the equations are summarized in the Table 2.4.

			Type of link	Equation in component notation
Displacement boundary conditions	$\hat{\mathbf{u}}$ - $\mathbf{u}$	on $S_{\hat{u}}$	strong	$u_i = \hat{u}_i$
Kinematic equations	$\mathbf{u}$ - $\boldsymbol{\varepsilon}^{\mathrm{u}}$	in V	strong	$\varepsilon^u_{ij} = \frac{1}{2}\left(\frac{\partial u_i}{\partial x_j} + \frac{\partial u_j}{\partial x_i}\right)$
	$\boldsymbol{\varepsilon}^{\mathrm{u}}$ - $\boldsymbol{\varepsilon}^{\sigma}$	in V	weak	$\int_V \left(\varepsilon^u_{ij} - \varepsilon^{\sigma}_{ij}\right) \delta\sigma_{ij}\, dV = 0$
Constitutive equations	$\boldsymbol{\varepsilon}^{\sigma}$ - $\boldsymbol{\sigma}$	in V	strong	$\varepsilon^{\sigma}_{kl} = E^{-1}_{ijkl}\sigma_{ij}$
Equilibrium equations	$\boldsymbol{\sigma}$ - $\mathbf{b}$	in V	weak	$\int_V \left(\frac{\partial \sigma_{ij}}{\partial x_j} + b_i\right) \delta u_i\, dV = 0$
Traction boundary conditions	$\boldsymbol{\sigma}$ - $\hat{\mathbf{t}}$	on $S_{\hat{t}}$	weak	$\int_{S_{\hat{t}}} (\sigma_{ij} n_j - \hat{t}_i)\, \delta u_i\, dS_{\hat{t}} = 0$

Table 2.4: Equations of the Hellinger-Reissner variational principle.

The contribution of the weak links yields:

$$\int_V \left(\varepsilon^u_{ij} - \varepsilon^{\sigma}_{ij}\right) \delta\sigma_{ij} dV - \int_V \left(\frac{\partial \sigma_{ij}}{\partial x_j} + b_i\right) \delta u_i\, dV + \int_{S_{\hat{t}}} (\sigma_{ij} n_j - \hat{t}_i)\, \delta u_i\, dS_{\hat{t}} = 0 \tag{2.19}$$

Following the alternations done in the previous sections in Equations 2.11 to 2.13, part of the second term of Equation 2.19 may be altered as:

$$-\int_V \sigma^u_{ij,j} \delta u_i\, dV = \int_V \sigma^u_{ij} \delta\varepsilon^u_{ij}\, dV - \int_S \sigma^u_{ij} n_j \delta u_i\, dS \tag{2.20}$$

By substituting back into equation 2.19, the volumetric integral terms (2.21) and the surface integral terms (2.22) are following:

$$\int_V \left(\varepsilon^u_{ij} - \varepsilon^{\sigma}_{ij}\right) \delta\sigma_{ij} dV - \int_V b_i \delta u_i + \int_V \sigma_{ij} \delta\varepsilon^u_{ij}\, dV + \tag{2.21}$$

$$\int_{S_{\hat{t}}} (\sigma_{ij} n_j - \hat{t}_i)\, \delta u_i\, dS_{\hat{t}} - \int_S \sigma_{ij} n_j \delta u_i\, dS = 0 \tag{2.22}$$

The variation of displacements δu_i is zero where kinematical boundary conditions are applied and the variation of stresses $\delta\sigma_{ij}$ is zero where traction is prescribed.

As described in the previous paragraph, $S = S_{\hat{t}} \cup S_{\hat{u}}$ and the function, in this case variation of displacements δu_i, is equal to zero on $S_{\hat{u}}$. By dividing the surface integrals, subtracting and eliminating the zero terms on $S_{\hat{u}}$, the following equations is obtained [12]:

$$\delta \mathrm{HR} = \int_V \left[\left(\varepsilon_{ij}^u - \varepsilon_{ij}^\sigma \right) \delta\sigma_{ij} - b_i \delta u_i + \sigma_{ij} \delta \varepsilon_{ij}^u \right] \, dV - \int_{S_{\hat{t}}} \hat{t}_i \, \delta u_i \, dS_{\hat{t}} = 0 \tag{2.23}$$

Which is the exact variation of the HR functional:

$$\mathrm{HR} = \int_V \left[\sigma_{ij} \varepsilon_{ij}^u - \frac{1}{2} \sigma_{ij} E_{ijkl}^{-1} \sigma_{kl} - b_i u_i \right] dV - \int_{S_{\hat{t}}} \hat{t}_i \, u_i \, dS_{\hat{t}} = 0 \tag{2.24}$$

In alternate notation as:

$$\mathrm{HR} = \int_V \left[\frac{1}{2} \sigma_{ij} (u_{i,j} + u_{j,i}) - \frac{1}{2} \sigma_{ij} \varepsilon_{ij}^\sigma - b_i u_i \right] dV - \int_{S_{\hat{t}}} \hat{t}_i \, u_i \, dS_{\hat{t}} = 0 \tag{2.25}$$

The first term contains the kinematic equation, while the second term is the complementary energy density $\mathrm{U}^* = \frac{1}{2} \sigma_{ij} \varepsilon_{ij}^\sigma$, which is calculated based on the stress master field.

As in the minimum potential energy principle, the principle (Equation 2.25) may be divided to the "internal" part, comming from deformation and the "external" part of applied traction and body forces. As in the displacement based formulation, the functional "reflects an energy state":

$$\begin{aligned} \mathrm{HR} &= \mathrm{HR}_{\mathrm{int}} - \mathrm{HR}_{\mathrm{ext}} \\ \mathrm{HR}_{\mathrm{int}} &= \int_V \left[\frac{1}{2} \sigma_{ij} (u_{i,j} + u_{j,i}) - \frac{1}{2} \sigma_{ij} \varepsilon_{ij}^\sigma \right] dV \\ \mathrm{HR}_{\mathrm{ext}} &= \int_V b_i u_i dV + \int_{S_{\hat{t}}} \hat{t}_i \, u_i \, dS_{\hat{t}} \end{aligned} \tag{2.26}$$

Mathematically, by variation of the HR functional δHR, a stationary point is obtained, which is the solution to a boundary value problem. Contrary to the minimum potential energy principle, where variation with respect to u_i yields, as the name suggest, pure minimum, the mixed-field variation results is a saddle point, also called min-max problem which requires special attention in ensuring stability of the formulation (see chapter 4) [1]. According to Tchonkova [12], one interpretation of the mixed formulation is that of a constrained minimization problem, where the contstraint is introduced via Lagrange multiplier in the equilibrium equations.

Chapter 3

Finite Element Method

In has been mentioned many times in the previous chapter, that weak formulation serve as a basis for the development of the Finite Element Method (FEM). The formulations have given possibilities to find an approximative solution to the boundary value problem. However, in the form of differential or partial differential equations (and equivalent statements), the weak forms are equivalent to that of the strong form and do not offer solution as of themselves [1]. The description of a deformation of a body is in this form continuous and as such, is only solvable via mathematical manipulation. If solved in this manner, the solution is exact, however, the exact solution many times may not even be obtainable and furthermore, the need for analytical (closed-form) solution also limits the scope of application for the required knowledge as well as the possibility of software implementation.

Althouth the present thesis is written only in the scope of small displacements, deformations and rotations, the same statement could be applied to solution of many other mathematial models encountered in physics, such as fluid dynamics [16], electromagnetism or heat conduction [8].

Alternative approach to the solution of the presented continuous equations is an effort to sought an approximation to the exact solution. A summary of approximative methods is given in the first section of the chapter for context. Subsequently followed by the description of the Finite Element Method.

3.1 Approximation methods

3.1.1 Weighted residual method

The solution to a general problem described by ordinary or partial differential equations may be approximated via linear combination of linearly independent functions defined over the whole domain. By solving for the appropriate combination parameters an approximate solution is obtained [1]. Unless stated otherwise, the definition was taken from [17].

Let us suppose that our problem is defined by an equation $Au = f$ where A is a linear differential operator, u is an unknown function defined in a domain Ω and f is a known

function. Boundary conditions may be inscribed on part of the boundary Γ as $Bu = r$, where r are the prescribed values, or on their variation as $Bu = q$, where q is the prescribed value of a derivative.

The approximative solution $\hat{u} \approx u$ to the problem may be represented as a set of linearly independent functions (Equation 3.1), which satisfy the boundary conditions (Equation 3.2 and 3.3) as:

$$u \approx \hat{u} = \psi + \sum_{i=1}^{n} a_i \phi_i \tag{3.1}$$

$$B\psi = r \tag{3.2}$$

$$B\phi_i = 0 \tag{3.3}$$

The function ψ is known and defined as any function which fullfills the prescribed values of boundary conditions (Equation 3.2) while functions ϕ_i are known and equal to zero on Γ where boundary conditions are prescribed (Equation 3.3). The latter are also often called test functions.

There are certain requirements imposed on the set of the test functions so that quality approximative solution is obtained. The set should consists of linearly independent functions, so that when the number of trial functions approaches infinity $n \to \infty$, the approximative solution $\hat{u}$ converges to the exact one u.

Multiple methods has been formulated throughout the years to obtain the unknown coefficients. Zienkiewicz mentions in [1] for example the point collocation method, the subdomain method or the Galerkin method.

Galerkin method Among the approaches to solve for the unknown coefficients in the weighted residual method described in the previous paragraphs, the Galerkin method is often mentioned as the stepping stone to the Finite Element process of discretization [1].

Recalling the example of the previous paragraphs, a so-called residual to the approximative solution (Equation 3.1) may be formulated (Equation 3.4), which has the following form after substituting the original equation [17]:

$$R = A\ \hat{u} - f \tag{3.4}$$

$$R = A\ \psi + \sum_{i=1}^{n} a_i A\ \phi_i - f \tag{3.5}$$

Using similar technique to the creation of weak form of differential equations outlined in section 2.2, the residual R may multiplied at each point by so-called weighing functions W_i and be summed over the domain Ω, in a weak form of a functional [1] as:

$$\int_{\Omega} W_j R d\Omega \tag{3.6}$$

If the number of weighing functions W_j, m, is the same as the number of test functions of the second term n, the equation permits to obtain the coefficients a_i via system of equations $\mathbf{Ka} = \mathbf{f}$ as:

$$K_{ij} = \int_{\Omega} W_j A\ \phi_i d\Omega \tag{3.7}$$

$$f_j = \int_{\Omega} W_j f d\Omega\ - \int_{\Omega} W_j A\ \psi d\Omega \tag{3.8}$$

To obtain the residual as the null function, the trial functions should be a complete set [18].

3.2 Discretization in the FEM

The discretization process of the FEM utilizes a particular choice of the functions ψ and ϕ_i, which are not defined over the whole domain, but instead only on parts of the domain. Additionaly, the integration performed to obtain the residual leading to the system of equations is performed locally on the relevant part of the domain. The part of the domain where a particular function is defined is, in the framework of the method, called element [1]. Since there is finite number of such elements, it gave name to the method.

The points dividing the domain into segments (elements) are conventionally called nodes, which in conjunction create the mesh [1].

It was already mentioned that to obtain a quality approximative solution which converges to the exact solution upon increasing the number of the functions, the set of functions should be a complete set [18]. Naturally, throughout the development of the method, various types of functions has been employed, for example Fourier series in [19]. In contemporary software and implementations, often a polynomial functions are employed [14]. There are three requirements for the trial functions to fulfill [1]:

1. **continuity**: each function has to be continuous on the domain,

2. **completeness**: the functions must be a complete set,

3. **linear independence**: none of the trial functions may be linearly dependent.

For illustration, and while reffering to the same problem which was described in previous pragraphs in one dimension (Equations 3.1 to 3.2), a set of simple polynomial functions may be defined in a following manner [1]:

$$\phi_i = N_i = \begin{cases} 0 & x < x_{i-1} \\ \frac{x - x_{i-1}}{x_i - x_{i-1}} & x_{i-1} \leq x < x_i \\ \frac{x_{i+1} - x}{x_{i-1} - x_i} & x_i < x \leq x_{i+1} \\ 0 & x > x_{i+1} \end{cases} \tag{3.9}$$

This particular set of functions is continuous in x (C_0, shown in Figure 3.1a), while their derivatives are only continuous on the respective domain of the function with discontinuities at nodes, that is piecewise continuous (Figure 3.1b). The functions are in the context of FEM referred to as shape functions. Generally, the approximative solution is obtained by addition of the shape function, while the same functions serve to obtain values in between nodes via interpolation [1].

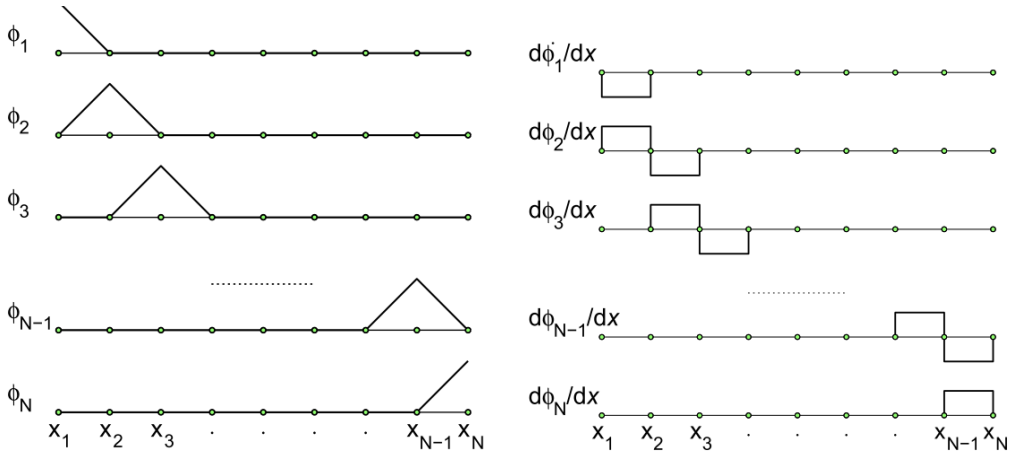

(a) C_0 continuous polynomial functions.

(b) Piecewise continuity of shape functions derivatives.

Figure 3.1: Shape functions of one-dimensional Finite Element Method example, graphs taken from [1].

The convergence of the solution was earlier conditioned by increase ofn the number of shape function. Given the definition of shape functions and the discretization they present, in the context of FEM it translates to increasing the number of nodes (and elements) in the mesh. The procedure is reffered to as h-refinement [20].

Alternatively, it is possible to increase the polynomial order of shape functions from $p = 1$ presented in Equation 3.9. As in the case of h-refinement, with higher polynomial order of the shape functions, the solution should converge to the exact solution. The procedure is called p-refinement [20]. The possibility of p-refinement which might be easily implemented is one of the advantages of the Finite Element Method [1].

As an example of such a refinement to the above shown function may serve the following graph, where shape functions for the bar element with polynomial order $p = 2$ are shown [2].

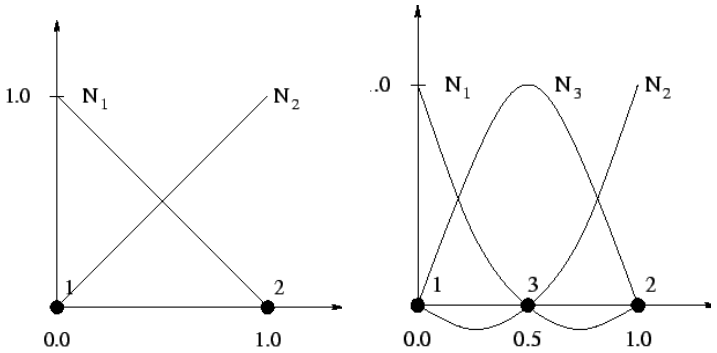

(a) $p = 1$ shape functions. (b) $p = 2$ shape functions.

Figure 3.2: p-refinement of the FEM, graphs taken from [2].

According to Zienkiewicz [1], one drawback of the procedure is the need of new computation, since the $p = 2$ polynomial order requires the use of different shape functions.

The shape functions are defined on the whole domain, but their value is non-zero only in parts of the domain, on respective elements. So the functions may be used in local coordinates for each element. The local coordinate system is often called natural with its axes being denoted (in three dimensions) by ξ, η and ζ. In case of the above shown 1D functions, in natural coordinate system they have the following form [17]:

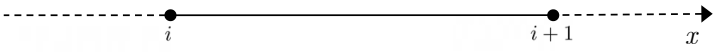

(a) I-th element in the global coordinate system.

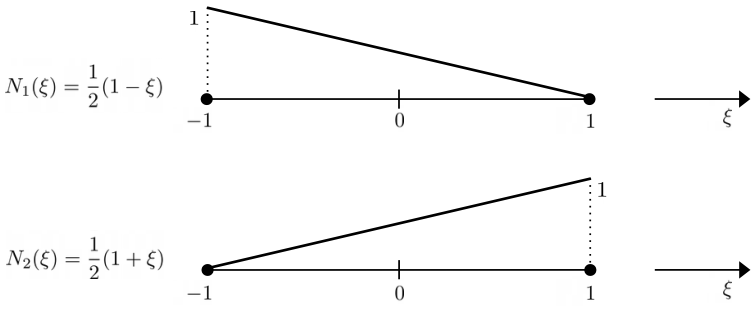

(b) Shape functions in natural coordinates of the same element.

Figure 3.3

The approximation of the solution in the natural coordinates then takes the following form [17]:

$$\hat{u}_i^e(\xi) = N_1(\xi)u_1^e + N_2(\xi)u_2^e, \qquad -1 \leq \xi \leq 1 \tag{3.10}$$

The superscript ^{e} denotes value in the local coordinate system. The values of shape function $N_1(-1) = 1$ and $N_1(1) = 0$, in case of the shape function N_2 the values are opposite in a sense that $N_2(-1) = 0$ and $N_2(1) = 1$. Subsequently, the values of the unknown coefficients u_i^e and u_{i+1}^e represent the value of function $\hat{u}^e$ in nodes which are obtained via linear combination of the two terms, as in Equation 3.10. Consequently, the nodal value of the approximatian in local coordinate system is equal to the global nodal values as $\hat{u}^e(-1) = u_i^e = u_i$ and $\hat{u}^e(1) = u_{i+1}^e = u_{i+1}$ [17]. Last but not the least, the use of ξ interval $-1 \leq \xi \leq 1$ facilitates the use of Gauss numerical integration, which may also be performed locally in the natural coordinate system [4].

Linear elasticity is only one of the field in which Finite Element Method is used as an approximation method [8]. The unknown parameters at nodes, here denoted by u_1^e and u_2^e in the local coordinates and by u_i and u_{i+1} in the global coordinates can represent various variables. In the context of the displacement based model of linear elasticity which was presented in section 2.2.1, the unknown parameters are an approximation to displacements, from which the strain and stress fields are derived [1]. In case of the latter formulation based on the Hellinger Reissner two-field variational principle, unknown parameters to represent both displacement and stresses are present [5]. Specifics of the implementations will be discussed in sections describing the particular elements: displacement based Q4 element in section 3.3 and the mixed principle based Pian-Sumihara element in section 3.4.

Isoporametric elements are elements in which the same shape functions are used to interpolate geometry between the nodes in global coordinates [1]. When mapping from the local coordinate system and vice versa, a one-to-one relationship is established between the two [17]. Remembering Equation 3.11, the relationship may be described as:

$$x^e = N_1(\xi)x_i^e + N_2(\xi)x_{i+1}^e \tag{3.11}$$

Generally, the two formulas for higher order polynomial shape functions might be generalized as [1]:

$$u^e \approx \hat{u}^e = \sum_a^n N_a(\xi)\hat{u}_a, \qquad \sum_a^n N_a = 1 \tag{3.12}$$

$$x^e = \sum_a^n N_a(\xi)x_a \tag{3.13}$$

The sum of shape functions equals to one, which is known as partition of unity [1].

In addition to the isoparametric formulation, there are also subparametric elements, for which the functions for geometry interpolation are of a lower degree than those of nodal

values approximation. Additionaly, the inverse may be used, giving rise to superparametric elements [21].

Numerical integration is an integral part to the computational process, which allows easy implementation to software solutions. Given the formulation of isoparametric elements and the local (also called parent [1]) coordinate system, the integration may be done in the local system instead of the global one [4].

In Finite Element Method, often a Gaussian quadrature is used because of it's straighworward implementation [1]. This type of numerical integration is also used throughout the thesis and is used interchangeably with the term numerical integration. Other types of numerical integration are presented for example in [18].

The numerical integrations allows a transformation between the summation in integral form and it's equivalent form, when function value in certain points is taken and multiplied by weights, given coefficients. In one dimension [21]:

$$\int_a^b f(\xi)d\xi \approx \sum_j w_j f(\xi_j) \tag{3.14}$$

where $f(\xi)$ is a function in the local coordinate system evaluated at a given point ξ_j, which is also called Gauss point (GP). The boundaries a and b are ξ values in the natural coordinate system. In the previously shown 1D element, $a = -1$ and $b = 1$, which is an advantage of using the local coordinate system - one can work with convenient values for the integration [21]. The numerical integration may not produce the exact value of the integral, hence the approximate sign $\approx$. According to Zienkiewicz [1], if used correctly, the accuracy is sufficient for use in the Finite Element Method.

The obtained value needs to be transformed to the global coordinate system to be used with other elements. Comming from the global formulation, the formula may be written as:

$$\int_i^{i+1} \mathbf{F}(x)dx = \int_{-1}^{1} \mathbf{F}(\xi)\,|J^e|\,d\xi \tag{3.15}$$

where the jacobian $|J^e|$ is derived from the one-to-one relationship between the geometry of local and global coordinates [17]:

$$dx = \left(\frac{1}{2}x_{i+1}^e - \frac{1}{2}x_i^e\right) d\xi \tag{3.16}$$

The equivalent operation in two dimensions will be explained in the following section, which describes a two-dimensional isoparametric element Q4.

3.3 The Q4 element

The Q4 element is one of the most commonly used two-dimensional isoparametric element in the Finite Element Analysis [1].

The shape functions are linear in both directions, so the element is bilinear. The element has 4 nodes, when applied to 2D elasticity problems each has two degrees of freedom (DOFs) assigned, so in a total of 8 DOFs. The unknown parameters are the displacements in each node, in two directions. The global displacement field consists of displacements inside each element, to which a structure is discretized. Per one element, the degrees of freedom are denoted as:

$$\hat{\mathbf{u}}^T = \{\, u_1, v_1, u_2, v_2, u_3, v_3, u_4, v_4 \,\}^T \tag{3.17}$$

The element makes use of the previously described concept of isoparametric element, so there is one-to-one relationship between the element in global coordinates and the local coordinates. Both are described in the following figures along with the degrees of freedom.

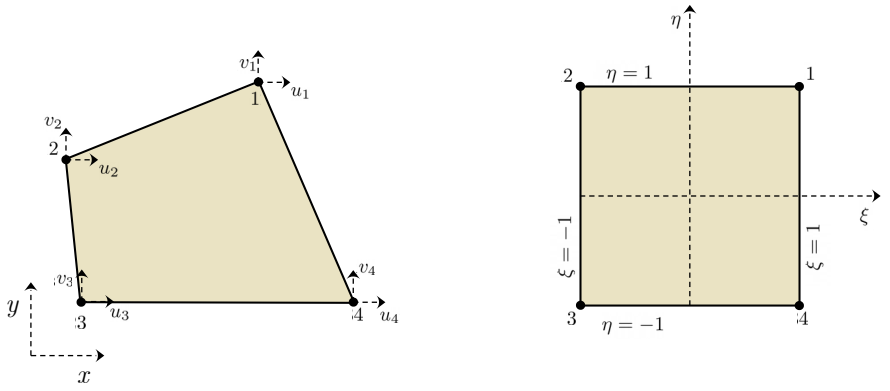

(a) Q4 element in global coordinate system.

(b) Q4 element in the parent, local coordinate system [1].

Figure 3.4: The Q4 element.

The shape function are [1]:

$$\begin{aligned} N_1 &= \frac{1}{4}(1+\xi)(1+\eta) \\ N_2 &= \frac{1}{4}(1-\xi)(1+\eta) \\ N_3 &= \frac{1}{4}(1-\xi)(1-\eta) \\ N_4 &= \frac{1}{4}(1+\xi)(1-\eta) \end{aligned} \tag{3.18}$$

The relationship between the nodal values, whether of displacements (Equation 3.19) or the geometry coordinates (Equation 3.20) is mapped via the same shape functions as [22]:

$$u = \sum_{a=1}^{n} N_a u_a, \qquad v = \sum_{a=1}^{n} N_a v_a \tag{3.19}$$

$$x = \sum_{a=1}^{n} N_a x_a, \qquad y = \sum_{a=1}^{n} N_a y_a \tag{3.20}$$

In the weak, variational form of Equation 2.18, all terms contain first derivative of displacements. Given the mapping between the global and local, natural coordinate system, derivatives of the shape functions in both systems and their relationship has to be defined [10].

For any function, including the shape functions, a chain rule is applied as:

$$\begin{aligned} \frac{\partial f}{\partial \xi} &= \frac{\partial f}{\partial x}\frac{\partial x}{\partial \xi} + \frac{\partial f}{\partial y}\frac{\partial y}{\partial \xi} \\ \frac{\partial f}{\partial \eta} &= \frac{\partial f}{\partial x}\frac{\partial x}{\partial \eta} + \frac{\partial f}{\partial y}\frac{\partial y}{\partial \eta} \end{aligned} \tag{3.21}$$

which might be written in matrix form as:

$$\begin{Bmatrix} \frac{\partial f}{\partial \xi} \\ \frac{\partial f}{\partial \eta} \end{Bmatrix} = \begin{bmatrix} \frac{\partial x}{\partial \xi} & \frac{\partial x}{\partial \eta} \\ \frac{\partial y}{\partial \xi} & \frac{\partial y}{\partial \eta} \end{bmatrix} \begin{Bmatrix} \frac{\partial f}{\partial x} \\ \frac{\partial f}{\partial y} \end{Bmatrix} \tag{3.22}$$

The matrix is known as Jacobi matrix, which is invertible as:

$$\frac{\partial \mathbf{f}}{\partial \boldsymbol{\xi}} = \mathbf{J}\frac{\partial \mathbf{f}}{\partial \mathbf{x}} \tag{3.23}$$

$$\frac{\partial \mathbf{f}}{\partial \mathbf{x}} = \mathbf{J}^{-1}\frac{\partial \mathbf{f}}{\partial \boldsymbol{\xi}} \tag{3.24}$$

where $\eta \equiv \xi_2$. The determinant of Jacobi matrix, the Jacobian was previously in one dimension denoted by J_e (Equation 3.15).

The general formula for numerical integration of any function in the natural 2D coordinate system is the following [10]:

$$\int_{-1}^{1}\int_{-1}^{1} f(\xi,\eta)d\xi d\eta = \sum_{j=1}^{n}\sum_{k=1}^{n} f(\xi_j,\eta_k)w_j w_k \tag{3.25}$$

Depending on the order of the polynomial function which is integrated, either a reduced or a full integration may be done [10]. The order of the numerical integration p_{ni} is given by

the number of points which are used in the integration. Full integration to obtain the exact solution is done in case that the polynomial degree of the function p is $p \leq 2p_{ni} - 1$. If the degree of a polynomial is higher, the result of the numerical integration is not exact and the procedure is reffered to as reduced integration [10].

Given the interval for both ξ and η where $-1 \leq \xi \leq 1$ and $-1 \leq \eta \leq 1$ (see Figure 3.4a), the coefficients w_j, also called weights, are given as:

order p_{ni}	number of GP	GP$_j$	weights w_j	note
1	1	$[0, 0]$	2	reduced integration
2	4	$[\pm\frac{1}{\sqrt{3}}, \pm\frac{1}{\sqrt{3}}]$	1	full integration

Table 3.1: Gauss points (GP) and weights for numerical integration of the Q4 element [1].

Reduced integration is an approach advantageous in certain aspects of Finite Element computations which will be further discussed at the end of the chapter.

Matrix form of the presented formulas is essential in allowing computer implementation of the Finite Element Method. The following section aims to give overview of the formulas, specific for the 4-node bilinear isoparametric quadrilateral of 8 degrees of freedom and derive the linear system of equations.

The uknown parameters of the system of equations are the approximated nodal displacemenets of an element given by vector of displacements denoted as $\hat{\mathbf{u}}$, the other uknown fields obtained subsequently from the displacement field are strain $\boldsymbol{\varepsilon}$ and stress $\boldsymbol{\sigma}$ fields, written respectively:

$$\hat{\mathbf{u}} = \{\, u_1, v_1, u_2, v_2, u_3, v_3, u_4, v_4 \}^T \tag{3.26}$$

$$\boldsymbol{\varepsilon} = \{\, \varepsilon_{xx}, \varepsilon_{yy}, \gamma_{xy} \,\}^T \tag{3.27}$$

$$\boldsymbol{\sigma} = \{\, \sigma_{xx}, \sigma_{yy}, \tau_{xy} \,\}^T \tag{3.28}$$

In matrix form, shape functions and shape functions derivatives are associated in matrices $\mathbf{H}$ and $\mathbf{B}$, respectively:

$$\mathbf{H}_i = \begin{bmatrix} N_i & 0 \\ 0 & N_i \end{bmatrix} \qquad \mathbf{B}_i = \begin{bmatrix} \frac{\partial N_i}{\partial x} & 0 \\ 0 & \frac{\partial N_i}{\partial y} \\ \frac{\partial N_i}{\partial y} & \frac{\partial N_i}{\partial x} \end{bmatrix} \tag{3.29}$$

Subsequently, it is possible to interpolate the nodal displacements $\mathbf{u}$ and obtain the strains from nodal displacements as:

$$\mathbf{u} = \mathbf{H}\hat{\mathbf{u}} \tag{3.30}$$

$$\boldsymbol{\varepsilon} = \mathbf{B}\hat{\mathbf{u}} \tag{3.31}$$

Stress at any point may be subsequently obtained via constitutive relation of plane stress or plane strain (Equations 2.7 and 2.8 repectively), denoted by $\mathbf{C}$, as:

$$\boldsymbol{\sigma} = \mathbf{C}\boldsymbol{\varepsilon} \tag{3.32}$$

The Equation 2.18 in 2D, where t is thickness of the structure equals to:

$$\int_S t\boldsymbol{\sigma}^u \delta\boldsymbol{\varepsilon}^u \, dS = \int_{S_{\hat{t}}} t\hat{\mathbf{t}}\delta\boldsymbol{u} \, dS_{\hat{t}} + \int_S t\mathbf{b}\delta\mathbf{u} \, dS \tag{3.33}$$

where $S_{\hat{t}}$ is the outline of the structure where traction $\hat{t}$. After substituting Equations 3.30 to 3.32 and altering the expression [10]:

$$\int_S t\mathbf{B}^T\mathbf{C}\mathbf{B} \, dS \, \hat{\mathbf{u}} = \int_{S_{\hat{t}}} t\mathbf{H}^T\hat{\mathbf{t}} \, dS_{\hat{t}} + \int_S t\mathbf{H}^T\mathbf{b} \, dS \tag{3.34}$$

The last equation defines the system of equations, which is notoriously known in the Finite Element Method:

$$\mathbf{K}\,\hat{\mathbf{u}} = \mathbf{f} \tag{3.35}$$

$$\mathbf{K} = \int_S t\mathbf{B}^T\mathbf{C}\mathbf{B} \, dS \tag{3.36}$$

$$\mathbf{f} = \int_{S_{\hat{t}}} t\mathbf{H}^T\hat{\mathbf{t}} \, dS_{\hat{t}} + \int_S t\mathbf{H}^T\mathbf{b} \, dS \tag{3.37}$$

Both matrix $\mathbf{K}$ and vector $\mathbf{F}$ are known, allowing to compute the unknown parameters, which are in this case nodal displacements.

Matrix $\mathbf{K}$ is known as the stiffness matrix, a symmetrical matrix describing the structure [23]. The order of the stiffness matrix of an element is equal to the number of degrees of freedom of the element, which is 8 for this particular element. The matrix is invertible when assembled for the global structure. If not, the structure undergoes a rigid body motion or is unconstrained [1].

Vector $\mathbf{f}$ is called load vector [1], through which, as the name suggests both traction and body force enter the linear system of equations.

Both stiffness matrix and load vector are usually evaluated locally making use of the local coordinate system along with the numerical integration and all their advantages, only to be localized into global stiffness matrix and load vector later on [1].

3.4 The Pian-Sumihara element

The previously described Q4 element is one of the simplest elements in two-dimensions. Shape functions are linear in both dimensions and the formulation is irreducible as only one primary field is present.

In situations where additional constraints are present, such as near incompressibility of a material, it may be convenient to include additional primary field resulting in mixed formulation (based on mixed principle principle as described in section 2.2.2) [10].

The Pian-sumihara element is based on the Hellinger-Reissner variational principle (summarized by Equation 2.25) and the concept of added internal incompatible displacements $\mathbf{u}_\lambda$ [24]. The displacement field of an element $\mathbf{u}_{\text{element}}$ consists of nodal displacements $\mathbf{u}$ and internal displacements $\mathbf{u}_\lambda$ as [5]:

$$\mathbf{u}_{\text{element}} = \mathbf{u} + \mathbf{u}_\lambda \tag{3.38}$$

After substituting the displacement field into the HR principle (Equation 2.25) in two dimensions, one obtains in matrix notation [24]:

$$\text{HR} = \int_S \left[t\,\boldsymbol{\sigma}(\mathbf{D}\mathbf{u} + \mathbf{D}\mathbf{u}_\lambda) - t\,\frac{1}{2}\boldsymbol{\sigma}\boldsymbol{\varepsilon}^\sigma - t\,\mathbf{b}\mathbf{u} \right] dS - \int_{S_{\hat{t}}} t\,\hat{\mathbf{t}}\mathbf{u}\,dS_{\hat{t}} = 0 \tag{3.39}$$

The displacements $\mathbf{u}$ are interpolated from nodal displacements $\hat{\mathbf{u}}$ via linear shape functions in both directions, as is geometry:

$$\hat{\mathbf{u}}^T = \{\, u_1\ v_1\ u_2\ v_2\ u_3\ v_3\ u_4\ v_4 \,\}^T \tag{3.40}$$

$$u = \sum_{a=1}^{n} N_a u_a, \qquad v = \sum_{a=1}^{n} N_a v_a \tag{3.41}$$

$$x = \sum_{a=1}^{n} N_a x_a, \qquad y = \sum_{a=1}^{n} N_a y_a \tag{3.42}$$

The internal displacements are given by four terms as [5]:

$$\begin{aligned} u_\lambda &= \lambda_1 \left(1 - \xi^2\right) + \lambda_2 \left(1 - \eta^2\right) \\ v_\lambda &= \lambda_3 \left(1 - \xi^2\right) + \lambda_4 \left(1 - \eta^2\right) \end{aligned} \tag{3.43}$$

The equations 3.43 may be substituted into the term containing the incompatible internal displacements of the HR functional (Equation 3.39) $\int_S t\,\boldsymbol{\sigma}\mathbf{Du}_\lambda\,dS$. After evaluating the integral in parent coordinates and further altering the expression (see [5] for full account of the procedure).

Subsequently, tensor stress equation may be also obtained when the basis vectors of natural coordinates are used [5]:

$$\begin{Bmatrix}\tau_{11}\\ \tau_{22}\\ \tau_{12}\end{Bmatrix} = \begin{bmatrix}1 & 0 & 0 & \eta & 0\\ 0 & 1 & 0 & 0 & \xi\\ 0 & 0 & 1 & 0 & 0\end{bmatrix}\begin{Bmatrix}\alpha_1\\ \alpha_2\\ \alpha_3\\ \alpha_4\\ \alpha_5\end{Bmatrix} = \begin{Bmatrix}\alpha_1+\eta\ \alpha_4\\ \alpha_2+\xi\alpha_5\\ \alpha_3\end{Bmatrix} \tag{3.44}$$

Normal stresses consist of constant and linear (bending) terms while shear remains constant [1]. To convert the tensor stresses into global coordinate system and thus obtain $\boldsymbol{\sigma}$, Jacobi matrix $\mathbf{J}_{(\xi,\eta)}$ evaluated in the center of an element $\mathbf{J}_{(0,0)}$ is used [1]:

$$\boldsymbol{\sigma} = \mathbf{J}^T_{(0,0)}\boldsymbol{\tau}\,\mathbf{J}_{(0,0)} \tag{3.45}$$

$$\begin{bmatrix}\sigma_{xx} & \tau_{xy}\\ \tau_{xy} & \sigma_{yy}\end{bmatrix} = \begin{bmatrix}J_{11} & J_{21}\\ J_{12} & J_{22}\end{bmatrix}\begin{bmatrix}\alpha_1+\eta\ \alpha_4 & \alpha_3\\ \alpha_3 & \alpha_2+\xi\alpha_5\end{bmatrix}\begin{bmatrix}J_{11} & J_{12}\\ J_{21} & J_{22}\end{bmatrix} \tag{3.46}$$

Evaluating the matrices, one finally obtains the expression for stress field as:

$$\begin{Bmatrix}\sigma_{xx}\\ \sigma_{yy}\\ \tau_{xy}\end{Bmatrix} = \begin{bmatrix}J_{11}^2 & J_{21}^2 & 2J_{11}J_{21} & J_{11}^2\eta & J_{21}^2\xi\\ J_{12}^2 & J_{22}^2 & 2J_{12}J_{22} & J_{12}^2\eta & J_{22}^2\xi\\ J_{11}J_{12} & J_{21}J_{22} & J_{11}J_{22}+J_{12}J_{21} & J_{11}J_{12}\eta & J_{21}J_{22}\xi\end{bmatrix}\begin{Bmatrix}\alpha_1\\ \alpha_2\\ \alpha_3\\ \alpha_4\\ \alpha_5\end{Bmatrix} \tag{3.47}$$

According to Zienkiewicz [1], the transformation needs to be such that:

1. constant stresses can be preserved in the global coordinate system and the formulation is stable,

2. the transformation is independent of the selected numbering of nodes in the global coordinate system (invariance requirement).

Matrix form of the formulation is again necessary to facilitate software implementation. The element is bilinear in its interpolation of geometry and nodal displacements, so the same matrix $\mathbf{H}$ containing the shape functions is used as in the case of Q4 element:

$$\hat{\mathbf{u}} = \{ u_1, v_1, u_2, v_2, u_3, v_3, u_4, v_4 \}^T \tag{3.48}$$

$$\mathbf{H}_i = \begin{bmatrix} N_i & 0 \\ 0 & N_i \end{bmatrix} \tag{3.49}$$

$$\mathbf{u} = \mathbf{H}\hat{\mathbf{u}} \tag{3.50}$$

The strains may be also obtained from the nodal displacements using the derivatives of shape functions grouped in matrix $\mathbf{B}$ as:

$$\mathbf{B}_i = \begin{bmatrix} \frac{\partial N_i}{\partial x} & 0 \\ 0 & \frac{\partial N_i}{\partial y} \\ \frac{\partial N_i}{\partial y} & \frac{\partial N_i}{\partial x} \end{bmatrix} \tag{3.51}$$

$$\boldsymbol{\varepsilon}^{\mathrm{u}} = \mathbf{B}\hat{\mathbf{u}}$$

Stresses are approximated independently via the basis vectors of the natural coordinate system. The transformation of Equation 3.45 may be directly included in matrix G to describe stresses as [1]:

$$\boldsymbol{\alpha} = \{, \alpha_1, \alpha_2, \alpha_3, \alpha_4, \alpha_5, \}^T \tag{3.52}$$

$$\mathbf{G} = \begin{bmatrix} J_{11}^2 & J_{21}^2 & 2J_{11}J_{21} & J_{11}^2\eta & J_{21}^2\xi \\ J_{12}^2 & J_{22}^2 & 2J_{12}J_{22} & J_{12}^2\eta & J_{22}^2\xi \\ J_{11}J_{12} & J_{21}J_{22} & J_{11}J_{22} + J_{12}J_{21} & J_{11}J_{12}\eta & J_{21}J_{22}\xi \end{bmatrix} \tag{3.53}$$

$$\boldsymbol{\sigma} = \mathbf{G}\boldsymbol{\alpha} \tag{3.54}$$

Strains of the stress field may also be easily computed by inverting the constitutive equation:

$$\boldsymbol{\varepsilon}^{\sigma} = \mathbf{C}^{-1}\boldsymbol{\sigma} \tag{3.55}$$

Substituting expressions for $\mathbf{u}$, $\boldsymbol{\varepsilon}^{\mathrm{u}}$, $\boldsymbol{\varepsilon}^{\sigma}$ and $\boldsymbol{\sigma}$ into the Equation 2.23 (δHR) one obtains [1]:

$$-\int_S t\,\mathbf{G}^T\mathbf{C}^{-1}\mathbf{G}\,dS\boldsymbol{\alpha}+\int_S t\,\mathbf{G}^T\mathbf{B}dS\hat{\mathbf{u}}+\int_S t\,\mathbf{B}^T\mathbf{G}\,dS\boldsymbol{\alpha}=\int_{S_{\hat{t}}} t\mathbf{H}^T\hat{\mathbf{t}}\,dS_{\hat{t}}+\int_S t\mathbf{H}^T\mathbf{b}\,dS \tag{3.56}$$

In may be conviniety rewritten similarly to the already described system of linear equations in case of Q4 element (Equation 3.35):

$$\begin{bmatrix}\mathbf{K_{11}} & \mathbf{K_{12}}\\ \mathbf{K_{21}} & \mathbf{0}\end{bmatrix}\begin{Bmatrix}\boldsymbol{\alpha}\\ \mathbf{u}\end{Bmatrix}=\begin{Bmatrix}\mathbf{0}\\ \mathbf{f}\end{Bmatrix} \tag{3.57}$$

$$\begin{aligned}\mathbf{K_{11}}&=-\int_S t\,\mathbf{G}^T\mathbf{C}^{-1}\mathbf{G}\,dS, \qquad \mathbf{K_{12}}=\int_S t\,\mathbf{G}^T\mathbf{B}dS, \qquad \mathbf{K_{21}}=\mathbf{K_{12}}^T\\ \mathbf{f}&=\int_{S_{\hat{t}}} t\mathbf{H}^T\hat{\mathbf{t}}\,dS_{\hat{t}}+\int_S t\mathbf{H}^T\mathbf{b}\,dS\end{aligned} \tag{3.58}$$

The integrals may be evaluated on element level in natural coordinates as previously described. The system described by Equation 3.57 may be reduced by static condensation [25] on the element level as well, not significantly burdening the computatioal process. The displacement part of the vector of uknown parameters $\hat{\mathbf{u}}$ is evaluated on the global level, while the uknown stress parameters are subsequently evaluated on the element level:

$$-\mathbf{K_{12}}^T{\mathbf{K_{11}}}^{-1}\mathbf{K_{12}}\,\hat{\mathbf{u}}=\mathbf{f} \tag{3.59}$$

$$\mathbf{K_{12}}^T\,\boldsymbol{\alpha}=\mathbf{f} \tag{3.60}$$

The shape functions of matrix $\mathbf{H}$ are still C^0 continuous (continuous functions with not continuous first derivatives), while functions of matrix $\mathbf{G}$ do not need to fulfill the continuity requirement [1].

3.5 Locking in Finite Element Method

There are particular situations in simulations where low order elements demonstrate excessive stiffness [26], resulting in the model returning undersetimated results or zero displacements. The behaviour is, among other elements, associated to the bilinear Q4 element which is an example of implemented low-order shape functions. Such behaviour is called locking phenomena [10].

The behaviour occurs in particular in two specific cases which are explained in the paragraph bellow.

(a) **Shear locking** occurs when spurious transverse shear strains occur, rendering the element incapable of representing bending dominated or other shear free behavior [27]. The phenomena is particularly associated with low-order isoparametric elements, because the deformation of an element is given by the elements geometry (Equations 3.19 and 3.20).

Figure 3.5 taken from [3] shows the mechanism of deformation in reality (Figure 3.5b) and as it is approximated by the bilinear quadrilateral element (Figure 3.5c). The wrong displacements result in spurious shear stresses and stresses in y direction (Figures 3.5d and 3.5e respectively).

As a result, the simulation shows conservative results in a stiffer behavior of the structure and returns smaller values of displacements [28].

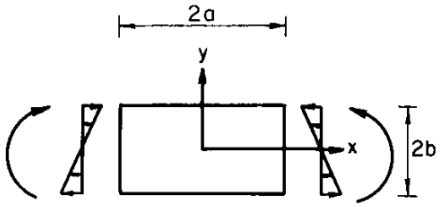

(a) Geometry, loading by bending moments and normal stress of a bilinear quadrilateral element.

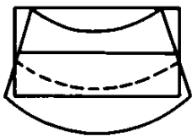

(b) Exact displacements.

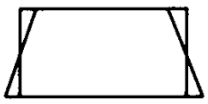

(c) Approximation by bilinear quadrilateral.

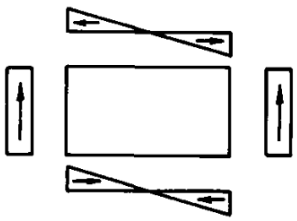

(d) Shear stresses occuring in the approximation (error).

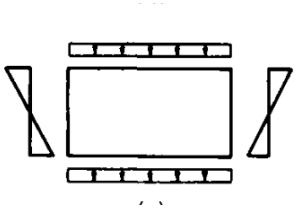

(e) Stresses in y direction.

Figure 3.5: Bending behavior approximation by quadrilateral bilinear element as taken from [3].

(b) **Volumetric locking** occurs when considering near incompressible material (that is when the value of Poisson's ratio $\nu \to 0.5$), the volume of the element is constant throughout the deformation. As such, no volumetric strain should be present, however, low order elements are not able to reproduce the non-existent volumetric strain, resulting in an overestimation of the elements stiffness and obtained displacements close to zero [29].

The requirement of incompressibility may be also stated as an constraint to the solutions, as it has to satisfy [6]:

$$\operatorname{div}(\mathbf{u}) = 0 \tag{3.61}$$

which limits the space of admissible solutions only to the subspace of incompressible deformation.

According to Babuška and Suri [30], in mathematical terms these problems are parameter dependent. In both cases, there is a physical parameter to the problem: in case (a) it is a beam's depth or a membrane thickness t while in case (b) it is the Poisson's ratio. The goal in developing mathematical formulations to solve the problems is to formulate a robust method such that the stability of the method and, subsequently, the results as well are parameter independent.

However, in low-order elements, locking occurs when the parameters value approaches to a limiting value, $t \to 0$ and $\nu \to 0.5$. The behavior will eventually disappear using finer mesh, which is what Babuška and Suri call "brute force" in [30]. Nevertheless, they also state that the required level of h-refinement may not always be feasible because of its computational demands, so multiple alternative approaches have been developed to overcome the phenomena [1]. The following paragraphs aim to summarize the methods for both shear locking and volumetric locking, since the approaches are similar or overlapping in many cases.

The locking phenomena is relevant primarily to the displacement based irreducible model. One technique in particular has seen success as a locking remedy (both shear and volumetric locking) and that is a selective reduced integration method.

It is possible to divide the consitutive matrix $\mathbf{C}$ into two parts, each describing different aspect to the deformation [4]:

$$\mathbf{C} = \mathbf{C}_{\mathrm{I}} + \mathbf{C}_{\mathrm{II}} \tag{3.62}$$

which subsequently allows to divide the stiffness matrix integral as well. Equation 3.36 becomes:

$$\mathbf{K} = \int_S t\, \mathbf{B}^T \mathbf{C} \mathbf{B}\, dS \tag{3.63}$$

$$= \int_S t\, \mathbf{B}^T \mathbf{C}_{\mathrm{I}} \mathbf{B}\, dS + \int_S t\, \mathbf{B}^T \mathbf{C}_{\mathrm{II}} \mathbf{B}\, dS \tag{3.64}$$

In case of shear locking, that would be a stiffness matrix describing the shear from Figure 3.5d as a separate term [3], in case of volumetric locking it would be the deviatoric stiffness matrix. Upon dividing the stiffness matrix integral it is possible to apply full integration to the first term and reduced integration to the shear/deviatoric term, a procedure dubbed as selective reduced integration (SRI) method. This approach has been successfuly applied in both shear [28] and volumetric locking. It is often applied on the Q4 bilinear element [4], However it may produce a stiffness matrix with directional properties [3].

Apart from selective reduced integration, also fully reduced integration has been suggested to calculate the complete term of stiffness matrix. Although correct solution may be obtained in certain cases, this approach leads to spurious kinematic zero energy modes, also known as hourglassing. These have been observed in the selective reduced integration, but to a smaller degree [26].

Another often mentioned remedy to locking is the use of mixed formulation [29] of multiple primary fields or added degrees of freedom in the form of incompatible displacements [26].

In the use of mixed/hybrid principles[1], one of the more prominent mixed elements in literature are based on the Hellinger-Reissner variational principle (described in section 2.2.2, consisting of two primary variables) or Hu-Washizu principle (approximating three fields independently, described to detail for example in [1] or [9]).

According to de Veubeke [15], mixed formulations are subjected to so-called *limitation principle* so the addition of stress variables does not necessarily improve the accuracy of the model. In Zienkiewicz's words, the principle states that:

> if the mixed formulation is capable of producing the same approximation of that produced by direct displacement form then it will in fact reproduce that form exactly and give identical and therefore not improved results [15, p. 289].

That is for example the case if the stress field is approximated by higher order polynomials than the displacement field [1].

The incompatible modes method aims to enhance the displacement field with internal degrees of freedom which are incompatible between elements (Figure 3.6) and thus allow better approximation of displacements [3]. The difference between compatible and incompatible mapping is conveniently illustrated by Felippa [4] in Figure 3.6:

[1] Mixed elements approximate multiple internal fields, while hybrid elements take one internal field and other field on the boundary of an element [10].

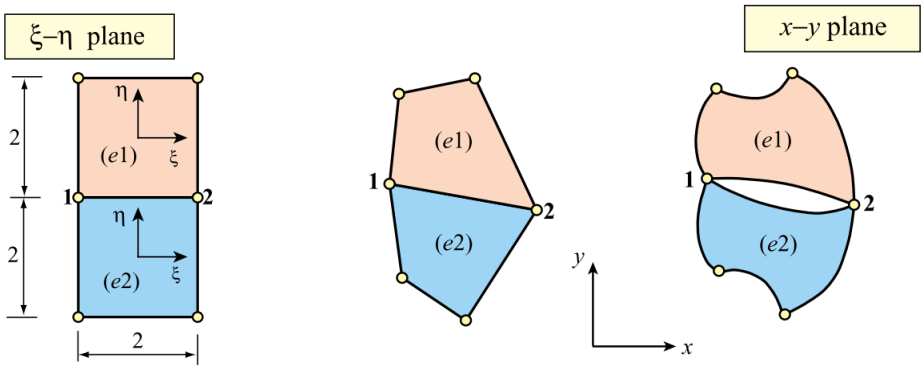

(a) Two elements in the natural coordinate system.

(b) Compatible mapping (left) and incompatible mapping (right) to the global coordinate system.

Figure 3.6: Compatible and incompatible mapping taken from [4].

The shape functions used to approximate both geometry and displacements are compatible in the Q4 element, as well as in case of the PS element. In the incompatible modes method, the incompatibility is applied on additional degrees of freedom to the displacement field [3]. In case of the Pian-Sumihara, the approximation of stress field may be incompatible [1].

Another possible approach to alleviate shear and volumetric locking is the enrichement of strain or stress internal fields, dubbed as a enhanced strain method [31, 32]. According to Simo and Rafai [33], the methods falls within the scope of mixed field methods, where in assumed strains the matrix $\mathbf{B}$ is extended with enhanced strains resulting in $\mathbf{B}$-bar similar method and an example of enhanced stress element is the Pian-Sumihara element based on displacement-stress mixed formulation.

Last but not the least, in the case of shear locking, higher order shape functions may alleviate the behaviour without completely eliminating it [34]. However, such an approach adds additional degrees of freedom on global level, increasing the CPU cost, in opposition to the mixed-field, incompatible modes and enhanced strain approaches, where the degrees of freedom may be eliminated on the element level by static condensation.

Chapter 4

Stability of the Finite Element Method and the patch test

In the Finite Element Method development throughout the years, an integral part to the advancement has been the validation and testing of the proposed solutions. According to Ziekniewicz [1], a finite element formulation should be such that both stability and consistency requirement is fulfilled. The former translates to a necessity of a unique solution with no spurious modes present, which may also be done by ensuring that the stiffness matrix K is "non-singular for all element assemblies" [1]. The latter requires that for elements size approaching zero $h \to 0$, the approximated discrete solution approaches to the exact solution (in a weak sense at least [35]). Bathe adds that the fact that a particular formulation is based on a variational principle does not ensure neither stability nor consistency [36].

Testing of a formulation should ensure that both of these requirements are fulfilled, but should in addition serve to the following purposes as well, as it more generally ensures [1]:

(a) convergence of a finite element formulation,

(b) assessment of a formulation's convergence rate,

(c) sufficient robustness of the implementation's algorithm,

(d) ensure correct formulation in case of incompatible modes elements,

(e) correct programming.

Throughout the years of FEM development, traditionally so-called patch tests have been used in finite element testing. First used by Irons in [37], the patch tests verifies that arbitrary assembly of finite elements is able to reproduce exact results of linear elastic body deformation upon loading by displacements consistent with constant straining [35]. Performing a patch test is a purely numerical procedure [38].

According to Zienkiewicz [1], the patch test may be applied to an assembly of any elements or to a single element, but there are certain elements which do not satisfy a single element patch test but an assembly of these elements does. Particularly relevant to this thesis is the applicability of the patch test to both irreducible and mixed methods.

It was mentioned in relation to the Hellinger-Reissner variational principle, that the mixed variational principles result in a saddle point problem, as one of the internal fields is essentialy a constraint enforced by a Lagrange multiplier [12]. Mathematical study of the convergence of such formulations has been done by Brezzi [39] and Babuška [40], resulting in formulation of the Babuška-Brezzi criterium which was accepted as a "condition for optimal performance of a method" [38].

In opposition to the patch test, the Babuška-Brezzi criterium is a theoretical framework to the assessment of finite element formulation, while the patch test is a test which may be also applied 'on inspection' [1] having the advantage of more straightforward application.

Certain ambiguity between the two approaches has been mentioned in literature as in some cases, the uniform inf-sup condition (the Babuška-Brezzi crierium) is not satisfied while the patch test is, for example in [38]. Babuška explains [38] that the criterium ensures optimal performance of a formulation when applied to a well defined set of data Λ. The inability of a method to satisfy the criterium doesn't exclude existance of a subset to the input data $\Lambda*$ where the patch test is satisfied along with the BB criterium.

In the scope of the thesis only the patch test will be performed as it is a sufficient condition to be met to assess formulation according to Ziekniewicz [1]. The following section will give theoretical overview of the methodology.

4.1 Patch test of the irreducible formulation

By the standard procedure, one obtains system of linear equations $\mathbf{K}\hat{\mathbf{u}} = \mathbf{f}$ which returns the approximated solution in the vector of unknown parameters $\hat{\mathbf{u}}$ upon evaluation. As it has been mentioned, the method leading to the system of equations should ensure both convergence and stability.

That is in the first case, the approximated solution $\hat{\mathbf{u}}$ obtained by the set of linear equations should approach the exact solution $\mathbf{u}$ as the size of the elements approaches zero. Mathematically [1]:

$$|\mathbf{u} - \hat{\mathbf{u}}| = O(h^q) \leq Ch^q \tag{4.1}$$

where h is the size of the element, C is a positive constant depending on the position and $q > 0$, which is the order of convergence in the variable $\mathbf{u}$.

Considering small domain of size $2h$ in two dimensions at point a, the solution $\mathbf{u}$ and the derivatives may be expanded in may be expanded via Taylor series. It is required that:

$$\begin{aligned}
\mathbf{u} &= \mathbf{u}_a + \left(\frac{\partial \mathbf{u}}{\partial x}\right)_a x + \left(\frac{\partial \mathbf{u}}{\partial y}\right)_a y + ... + O(h^p) \\
\frac{\partial \mathbf{u}}{\partial x} &= \left(\frac{\partial \mathbf{u}}{\partial x}\right)_a + ... + O(h^{p-1}) \\
\frac{\partial \mathbf{u}}{\partial y} &= \left(\frac{\partial \mathbf{u}}{\partial y}\right)_a + ... + O(h^{p-1})
\end{aligned} \tag{4.2}$$

with $p \geq 2$, so the approximation, as $h \to 0$, should result in the exact solution.

Taylor at al. [35] described two forms of the patch test to test the convergence. In form A, one takes a problem for which the exact value(s) of the vector $\hat{\mathbf{u}}_a$ is known and inserts it to the linear system of equations, to verify that:

$$\mathbf{K}_{ab}\hat{\mathbf{u}}_a - \mathbf{f}_b \equiv 0 \tag{4.3}$$

in this case, vector $\mathbf{f}$ introduces body force if any is present. Visual representation of the patch test may be in Figure 4.1a.

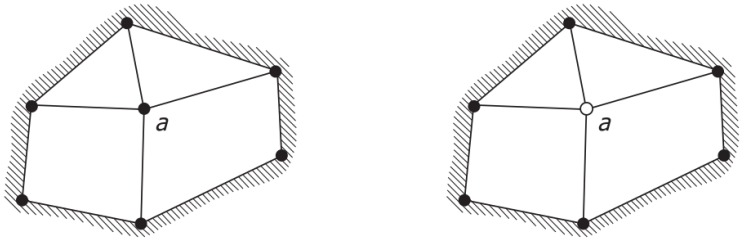

(a) Form A patch test. (b) Form B patch test.

Figure 4.1: Visual representation of the patch test as taken from [1].

Form B patch test, only values on the boundary of the assembly $\mathbf{u}_b$ are inserted and parameters in point a are obtained as:

$$\hat{\mathbf{u}} = \mathbf{K}_{aa}^{-1}(\mathbf{f}_a - \mathbf{K}_{ab}\hat{\mathbf{u}}_b), \qquad a \neq b \tag{4.4}$$

Visual description of the patch test taken from [1] is shown in Figure 4.1b.

For linear problems, where the uknown vector is obtained by $\hat{\mathbf{u}} = \mathbf{K}^{-1}\mathbf{f}$ the stability condition translates to the necessity of stiffness matrix $\mathbf{K}$ being non-singular for arbitrary element assembly. Apart from the patch test, the stability condition (i.e. the stiffness matrix) may be also verified separately [1]. This condition may be verified by a generalized patch test of form C, also described by Taylor et al. [35].

In the thrid and final form of the patch test for irreducible elements, minimum essential boundary conditions are applied to the assembly so that rigid body motion is eliminated and natural boundary conditions in form of traction are applied at the boundary of the assembly (see Figure 4.2). A solution at point a is obtained and compared to the exact solution.

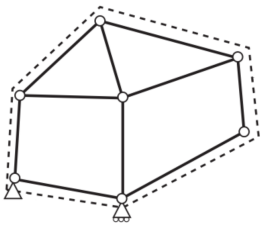

Figure 4.2: Generalized patch test of form C [1].

The vector $\mathbf{f}$ contains traction, the natural boundary conditions, so any singularity may be observed [1].

The test applied on an assembly of elements may not, on occasion, reveal instabilities, in opposition to the single-element patch test of the same form (Figure 4.3) which is according to Zienkiewicz [1] "one requirement of a good finite element formulation". However, there are certain cases of well documented elements, such as bilinear element Q4 and quadratic quadrilateral with 8 nodes (Q8), which are commonly used in the FEM [14] but do not satisfy the single-element patch test (the patch test is satisfied for the assembly of 2 and more elements).

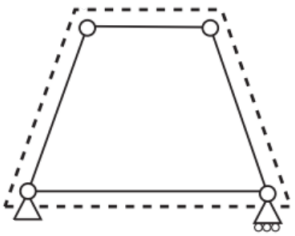

Figure 4.3: Single-element patch test [1].

4.2 Patch test generalized to mixed formulations

In the mixed formulation, there is a necessary, although not sufficient condition concerning the number of degrees of freedom in the vector of unknown parameters. Applied to the mixed formulation of $\boldsymbol{\sigma} - \mathbf{u}$, where n_α is the number of degrees of freedom (DOFs) associated to stresses while n_u is the number DOFs associated with displacements, the condition states that [1]:

$$n_\alpha \geq n_u \tag{4.5}$$

The condition has to be satisfied for a single element as well as for any assembly of elements or the whole structure.

Recalling the Equations 3.48 and 3.52 and applying essential boundary conditions as necessary supports to avoid rigid body motion $n_u = 8 - 3 = 5$, $n_\alpha = 5$ as the stress parameters are never constrained [41], so the above written equation is satisfied.

Chapter 5

Implementation and validation

The present section aims to first describe the implementation which was done in the context of the thesis, namely the algorithm of Finite Element Method solver with two implemented elements, followed by valiadtion of the implementation, a patch test and comparison of results of the present implentation to results obtained in literature.

5.1 Present implementation

For the purpose of the thesis a finite element method procedure to solve idealized 2D linear elasticity examples of plane strain or plane stress was developed in Python programming language [42] using Numpy [43] library in the solver and Matplotlib [44] library in post-processing. Flowchart of the script is shown below.

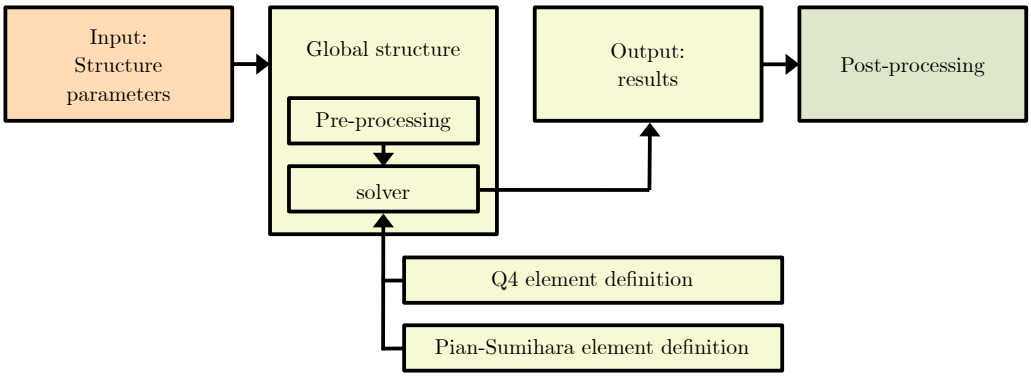

Figure 5.1: Flowchart of the implemented algorithm.

The structure is specified in the input file, including loading and boundary conditions. Subsequently, the geometry is discretized into nodes creating mesh in the pre-processing stage, which is then submitted to the solver. The implementation allows h-refinement, that is increasing the number of nodes to increase the model's accuracy, allowing to obtain converging solution. The p-refinement, that is increasing the order of shape functions [20],

was not implemented. All the simulations are done with linear shape functions (of order p=1) and full integration rule is used.

The solver incorporates two elements, the bilinear quadrilateral element described in section 3.3 and the Pian-Sumihara element described in section 3.4. It computes local stiffness matrix depending on the chosen element, followed by a global stiffness matrix of the structure. Boundary conditions are applied in form of prescribed displacement or traction in specific nodes and finally, vector of unknown parameters is computed and unknown vector / tensor fields are obtained. The global and desired local results (such as in a specific point) as well as desired graphic representation of the results are saved. In the final stage, separate script is used in post-processing to compare results.

5.2 Patch test

First in a series of tests aiming to validate the implemented solution is a simulation of a plate under uniaxial tension. Given that the displacement field in both directions is constant, when loading the plate by prescribed displacement the exact nodal displacement field is known beforehand and the patch test of form A as described in section 4.1 may be performed, assesing the difference of results obtained by the algorithm and the exact solution. The constant distribution of displacements may be also observed in a graph. The geometry of the patch test was chosen based on the patch test used by Nguyen and Ibrahimbegovic in [45].

The primary aim of the test is the validation of implementation of both Q4 element and Pian-Sumihara (PS) elements so the same test is applied to both. A plate of a given geometry is subjected to uniaxial tension of a given magnitude while the mesh consists solely of orthogonal elements. Subsequently, the mesh is distorted by a random factor of a given interval, creating irregular mesh. Both regular and irregular elements are expected to yield the same linear dependence of displacements on position. The difference between exact nodal displacements and computed results is assessed by obtaining standard deviation of the differences and subsequently the distribution is also verified in a graph.

Geometry of the plate and the material characteristics were selected following (in a consistent system of units):

Regular mesh was chosen to be 10x10 elements, in total 100 elements (Figure 5.3a). For second case, each inner nodal coordinate is changed randomnly as depicted in Figure 5.3b. The element's length l_{el} is multiplied by an arbitrary coefficient $c \in [-0.3, 0.3]$, which is added to the original nodal coordinates in orthogonal mesh in each direction.

Four configurations were tested in total. Resulting displacement fields are shown on the following figures, each linked to the respective case from the list.

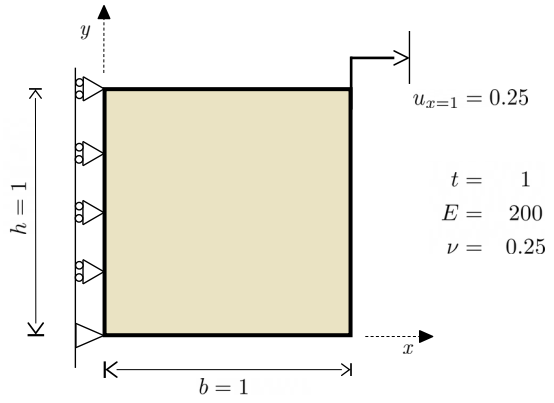

Figure 5.2: Geometry and material characteristics.

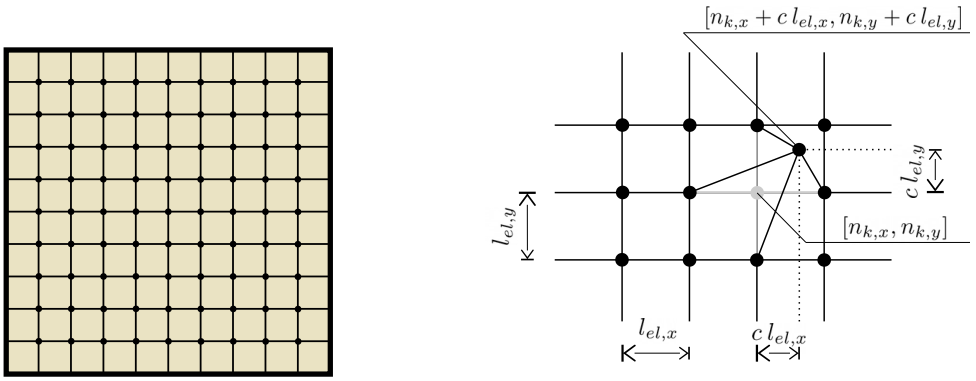

(a) Regular mesh.

(b) Example of a mesh disruption from regular (grey node) to irregular.

Figure 5.3: Mesh of the present patch test.

(a) Q4 element with regular mesh (Figure 5.4),

(b) Q4 element with disturbed mesh (Figure 5.5),

(c) PS element with regular mesh (Figure 5.6),

(d) PS element with disturbed mesh (Figure 5.7).

For each of the four cases, the exact nodal displacement of each inner node (node without prescribed displacement in considered direction) was obtained as:

$$u_n = \frac{u_{x=1}}{b} x_n, \qquad v_n = -\frac{\nu u_{x=1}}{h} y_n \tag{5.1}$$

where u_n and v_n are the exact values of nodal displacement in x and y direction respectively, $u_{x=1}$ is the value of prescribed displacement at the right edge, ν is the Poisson's

coefficient, b and h are structure's dimensions and x_n and y_n are coordinates of the considered node.

Standard deviation (SD) is computed for the error between exact solutions u_n, v_n and obtained solutions $\hat{u}_n, \hat{v}_n$ in all inner nodes as [18]:

$$\mathrm{SD}_u = \sqrt{\frac{\sum(u_n - \hat{u}_n)^2}{n}}, \qquad \mathrm{SD}_v = \sqrt{\frac{\sum(v_n - \hat{v}_n)^2}{n}} \tag{5.2}$$

where n is the number of inner nodes for which the standard deviation is obtained.

Following table summarizes the results for each of the four cases:

	case (a) Q4, regular mesh	case (b) Q4, disturbed mesh	case (c) PS, regular mesh	case (d) PS, disturbed mesh
SD_u	0.0	0.0	0.0	0.0
SD_v	$7.425\mathrm{e}^{-16}$	$5.135\mathrm{e}^{-16}$	$6.169\mathrm{e}^{-15}$	$9.298\mathrm{e}^{-16}$

Table 5.1: Standard deviation of differences between exact solution u_n, v_n and obtained results $\hat{u}_n, \hat{v}_n$.

In all case in the direction of prescribed displacement, the standard deviation is equal to zero, or rather smaller than the limiting precision in Python programming language which is e^{-18}.

In the opposite direction in all cases the standard deviation of error is obtainable, however, values of order e^{-15} to e^{-16} may be attributed to machine precision and furthermore are irrelevant in comparison to the magnitude of prescribed displacements. The patch test may be considered as succesful.

Subsequent figures show the distribution of displacements in both directions for all cases.

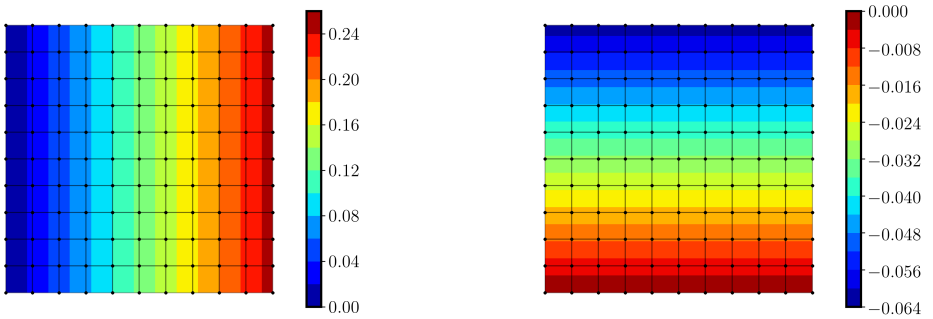

(a) u displacements. (b) v displacements.

Figure 5.4: Resulting displacement fields for regular mesh of Q4 elements.

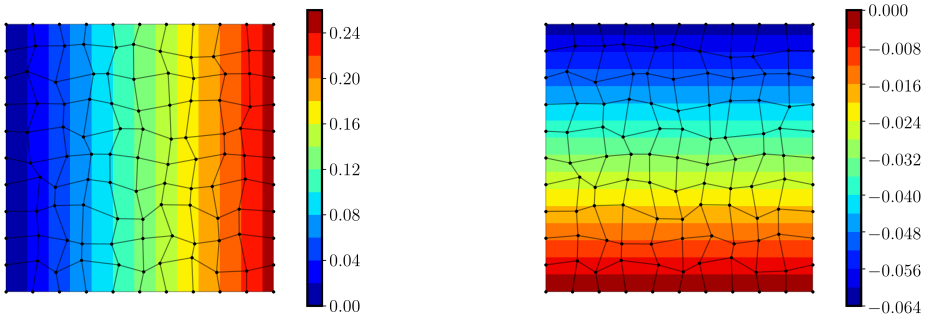

(a) u displacements. (b) v displacements.

Figure 5.5: Resulting displacement fields for irregular mesh of Q4 elements.

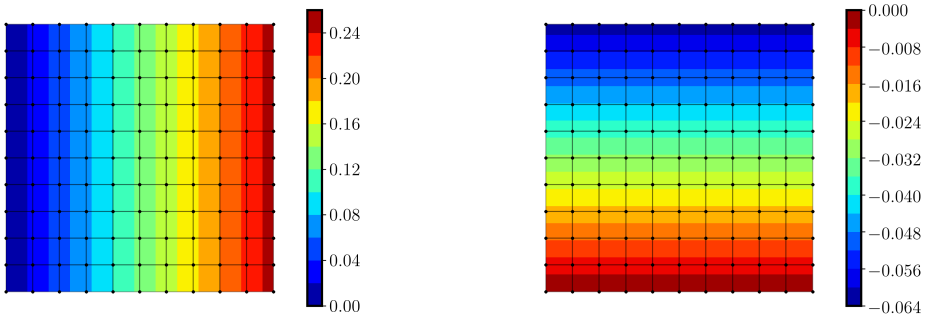

(a) u displacements. (b) v displacements.

Figure 5.6: Resulting displacement fields for regular mesh of PS elements.

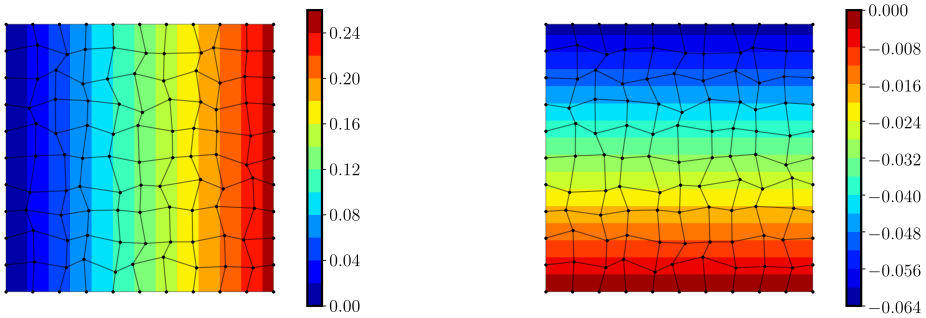

(a) u displacements. (b) v displacements.

Figure 5.7: Resulting displacement fields for irregular mesh of PS elements.

Irespectively of the regularity of the mesh or the type of element used, the same results are obtained: linear dependence of displacements on position in the plate in both direc-

tions. The distribution of strains as well as stresses are constant over the domain in both directions, while shear components are zero.

The results shown above thus met the expectations and show the implementation to be robust enough to succesfully obtain the correct results.

5.3 Uniaxial tension and bending

Upon proposal of the assumed stress element by Pian & Sumihara in [5], the element was also tested in multiple situations to assess its behaviour in comparison to other incompatible or hybrid elements. Also the Q4, as one of the most common quadrilateral elements, was included.

To test the present implementation of both Q4 and PS elements in different scenarios than unixial tension, the same simulations were run and results compared. The test cases (TC) along with results from in [5] and here obtained by the present implementation are compared and assessed.

Two geometries with different loading are tested as described on the following figures (dimensions and material characteristics are in a consistent system of units).

For the test case (a), horizontal displacement at point A u_A is compared. In test case (b), a vertical displacement of the same point v_A is investigated. The console loaded by bending moment of test case (c) as well as the same console loaded by traction of test case (d) are compared based on the vertical displacement in point a v_A and normal stress at point B $\sigma_{x,B}$.

The obtained results are summarized in Table 5.2, where also the results published in [5] are written. The table is completed by exact solution for each test case taken from the same source.

	TC(a)	TC(b)	TC(c)		TC(d)	
	u_A	v_A	v_A	$\sigma_{x,B}$	v_A	$\sigma_{x,B}$
Q4, [5]	6.00	-17.00	45.70	-1 761	50.70	-2 448
PS, [5]	6.00	-17.64	96.18	-3 014	98.18	-4 137
Q4, computed	6.00	-17.00	45.65	-1 761	50.96	-2 448
PS, computed	6.00	-17.64	96.18	-3 014	98.05	-4 073
exact solution [5]	6.00	-18.00	100.00	-3 000	102.60	-4 050

Table 5.2: Comparison of results.

For the first two cases, the obtained results do not differ. TC(a) is a case of uniaxial tension and results obtained with both elements are the exact solution. In TC(b) (bending) the results of the article and the obtained results are equal. The use of irreducible displacement based model shows slightly worse results than those of the PS element, which

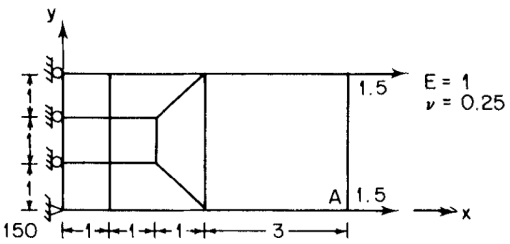

(a) Test case a: uniaxial tension.

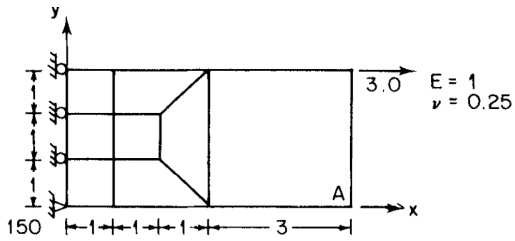

(b) Test case b: console loaded by a force inducing bending.

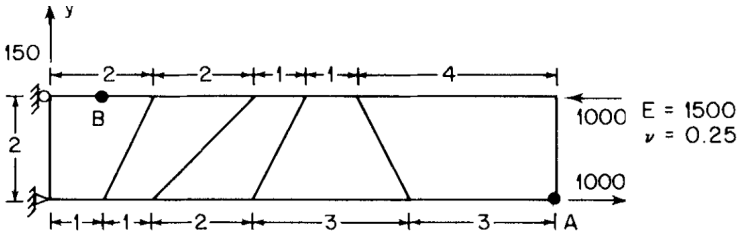

(c) Test case c: console with one disturbed element along the second dimension loaded by bending moment.

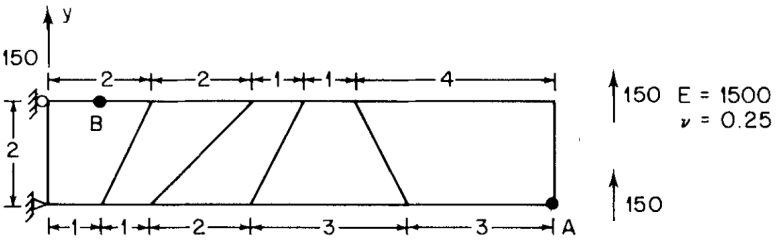

(d) Test case d: console with one disturbed element along the second dimension loaded by traction.

Figure 5.8: Variants of the test case taken from [5].

is given by the added unknown stress parameters in the latter case. As a result, the PS element shows better behaviour in bending in comparison to the Q4 element.

The same behavior may be observed with TC(c), where the difference between the results when comparing the two elements is even greater. While the results of PS element for both displacement v_A and stress $\sigma_{x,B}$ are approaching to the correct solution, the Q4 element shows results nowhere near the correct ones. Interestingly enough, in the results obtained by PS element, displacement v_A is slightly underestimated while stress in point B is computed slightly higher that the exact result, being on the safe side for design. The difference between results of different elements are more prominent than the previous test case (TC(b)) which also describes bending. One possible explanation is that in TC(b) there are more elements along the height of the beam in one half of the beam, than in the geometry of TC(c). These elements of TC(b) are thus able to capture bending better and subsequently show less of a difference in results between elements than in TC(c).

There are marginal differences between the computed results and those from [5] and as

obtained by the present implementation. The differences are attributed to the rounding error during computation, as both hardware and sotware used for the computation likely differes significantly.

The fourth test case TC(d) displays the same behaviour as in the previous TC. Slight differences may be observed between the two implementations as before and PS element shows much better behavior than the Q4 elements. The results are approaching the exact solution in a similar manner, with stress $\sigma_{\mathrm{x,B}}$ being on the safe side.

As described above, only small differences may be observed between the results, concluding test to be succesfull and validating the implementation by duplicating the results.

Chapter 6

Analysis of elements behavior

6.1 Distortion effect

Important part of any finite element development is the assesment of element's sensitivity to distortion [46]. The PS elements possesses higher number of DOFs than the Q4 element (13 and 8 respectively), so it is desirable that the element would be effective for small number of elements. Subsequently, it would be possible to keep the computational cost low even though higher number of DOFs is present.

Possible test to see the effect of element distortion to the results was proposed by Pian and Sumihara in [5]. The test consists of subjecting a console to bending, while the mesh consists of two elements. These vary shape from rectangular to highly distorted so the effect on the results may be observed. The amount of distortion is represented by a parameter a, which is the dimension by which an element is distorted (that is the amount by which a node is displaced), see Figure 6.1.

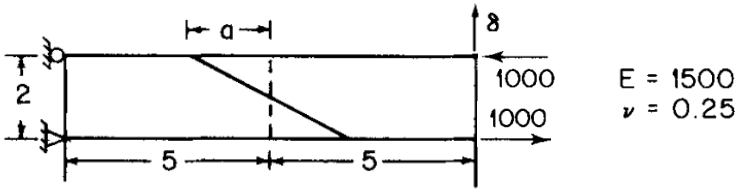

Figure 6.1: Geometry and material characteristics of the distortion effect test.

The geometry and loading are the same as in case TC2(c) of section 5.3, in a consistent system of units. Full integration is implemented. Coarse mesh of two elements is used. In this case, results are plotted as a percentage of the correct solution (0% error is the correct solution). In absolute value the exact solution is $v_A = 100$ (see Table 5.2).

Results of the analysis are displayed in Figure 6.2. Each color represents one type of element. Dashed line is the result obtained by Pian and Sumihara in [5] while solid line represents the result obtained by the present algorithm. The two differ marginally, likely

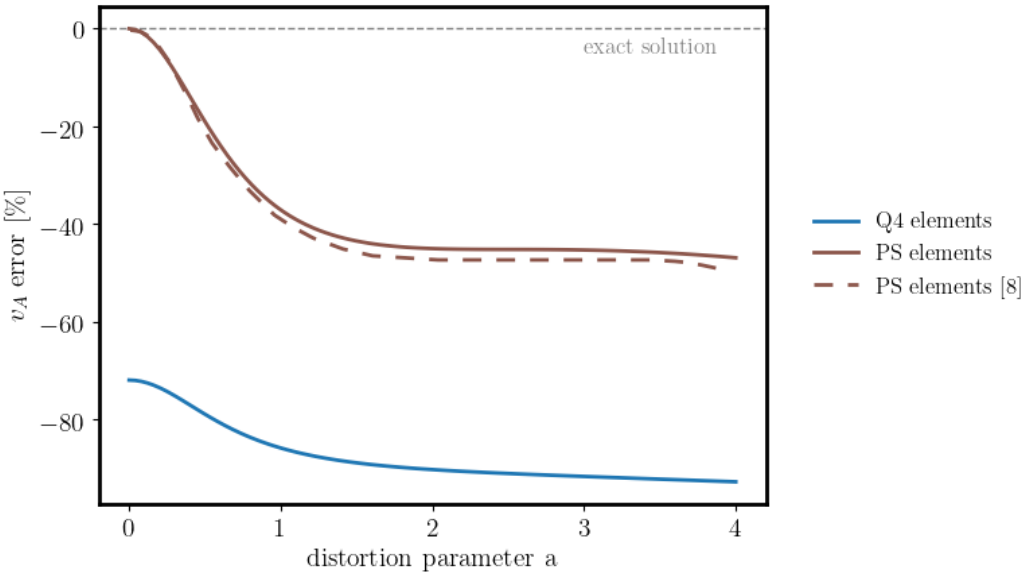

Figure 6.2: Results of the convergence analysis, dashed line represents results taken from [5].

because of a low quality graph of the original published results (slight distortion in print). The difference is considered insignificant.

The graph shows differences between the elements. While two rectangular elements of the PS element are able to capture the bending precisely, the Q4 element shows about error 70%. By starting to distort the element, there is a fall until $a = 1$ for both elements. Subsequently, the effect of further distortion stabilizes in both cases for distortion greater than $a = 2$.

While the behavior of the Q4 and the PS element is not comparable in terms of results, the element's the distortion effect to both is largely similar. In both cases best results are obtained by non distorted elements, followed by a decline and subsequent stabilization of the quality of result for greater distortion.

It is worth noting, that the PS element is able to capture pure bending behaviour of the beam extremenly well. With only two rectangular elements along the length of the beam and one element along the depth of the beam, the exact solution is obtained.

6.2 Convergence analysis

Another important aspect of any finite element is its efficiency. The present anlysis was done based on the analysis performed by Nguyen and Ibrahimbegovic in [45]. The aim is to compare performace of the two elements in pure bending state and compare convergence rate. Additionaly, in the analysis of Nguyen Q4 element is tested, so the analysis partly serves for validation of the element implementation. PS element is added and further analysis of strain fields is done for elements to better understand behavior of the elements.

The pure bending convergence is examined on a simply supported beam loaded by bending moment at both ends. For the purpose of a comparison, vertical displacement of the middle point on the upper edge $v_{M[5,1]}$ is of interest. Full integration is used. The exact solution was taken from [45]. See the Figure bellow for geometry and material characteristics in consistent system of units. The beam is modelled in plane strain with thickness $t = 1$.

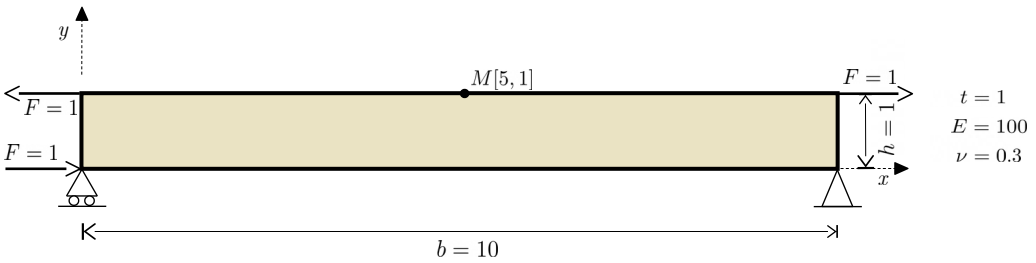

Figure 6.3: Geometry and material characteristics of the test case for convergence analysis.

In the first part, the following mesh density is tested (number of elements in x direction and number of elements in y direction): 6x1, 12x6, 24x12, 36x12, 72x24. Exact solution is equal to $v_{M[5,1]} = 1.522$ Following results were obtained.

mesh elements	6x1	12x6	24x12	36x12	72x24
PS element	1.500	1.503	1.509	1.513	1.521
Q4 element	0.400	0.887	1.283	1.401	1.488

Table 6.1: Results of the convergence analysis, exact result of the vertical displacement is equal to $v_{M[5,1]} = 1.522$.

The graph in Figure 6.4 shows resulting displacement $v_{M[5,1]}$ for each mesh configuration of the two elements, numerical results are written in the Table 6.1 above. For the coarsest mesh (6x1 elements), the displacement obtained with PS element is approaching the exact solution. The Q4 element displacement obtained with Q4 element is equal to $v_{Q4,6x1} = 0.4$. It clearly shows, that the mesh configuration of Q4 element doesn't possess enough degrees of freedom to capture the behavior of the beam.

By refining the mesh of PS elements, only minor improvement is obtained. the solution of the coarsest mesh is already close to the exact solution so mesh refinement doesn't bring about significant difference in the resulting displacement. Furthermore, the minor improvement doesn't justify the added computational cost to the analysis.

In the case of Q4 element, mesh refinement has significant impact on the quality of the model. Nevertheless, although the improvement is significant and the solution is converging ($v_{Q4,6x1} = 0.400$,$v_{Q4,12x6} = 0.887$, $v_{Q4,12x24} = 1.283$ and $v_{Q4,12x24} = 1.401$)

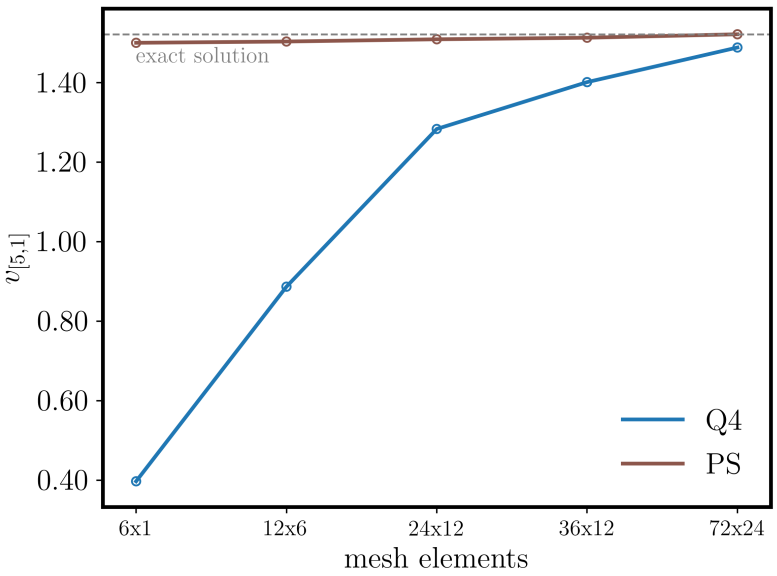

Figure 6.4: Graph of the convergence analysis results.

only the solution obtained by the finest mesh of 1728 elements $v_{Q4,12x24} = 1.488$ approaches to the exact solution. The lack of DOFs in the element definition needs to be compensated with large number of elements (thus increasing the overall number of DOFs), increasing the computational cost rapidly.

However, even the finest mesh of Q4 elements doesn't exceed the quality of solution obtained by the coarsest mesh of PS elements.

Second part of the analysis aims to compare strain fields of the elements. There are three fields to test for each mesh configuration:

(a) $\boldsymbol{\varepsilon}_{Q4}$: strain field obtained by the Q4 element,

(b) $\boldsymbol{\varepsilon}^{\mathrm{u}}_{\mathrm{PS}}$: strain field obtained by the PS element via kinematic equations from displacement field,

(c) $\boldsymbol{\varepsilon}^{\boldsymbol{\sigma}}_{\mathrm{PS}}$: strain field obtained by the PS element via inverted constitutive equation from stress field.

To allow numerical comparison of the results, instead of comparing the whole strain field for each case, only specific sections of the structure are compared in a graph. These sections were chosen to best represent possible deviations between the fields in areas of the highest tension / compression. Three sections are compared, each describing different strain component. The deformed shape is showed in Figure 6.5, followed by depiction of the sections, which will be compared in Figure 6.6.

The following two graphs shows the strains obtained via different fields. Strains obtained by the Q4 element (via displacement field) are depicted by solid lines, those obtained

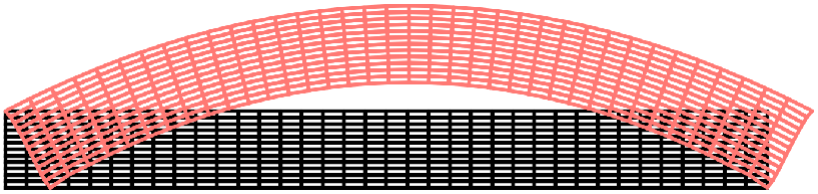

Figure 6.5: Deformed shape of the beam obtained with PS element and 36x12 mesh.

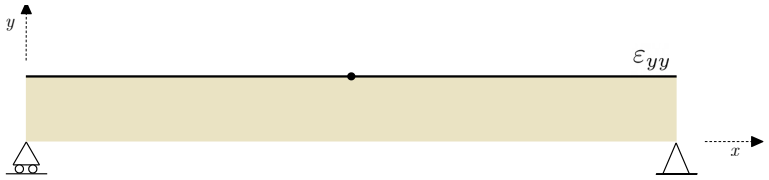

(a) Section for ε_{yy} comparison.

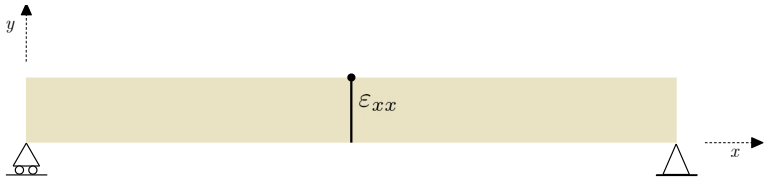

(b) Section for ε_{xx} comparison.

Figure 6.6: Sections for strain field comparison.

by the PS element via displacement field are plotted with dashed line and those obtained via stress field are dotted.

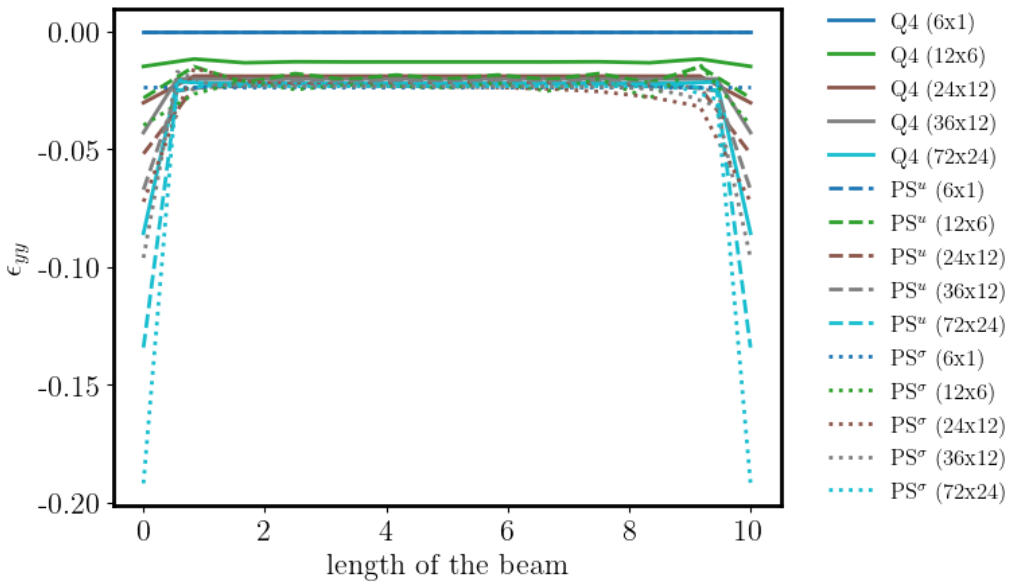

Figure 6.7: ε_{yy} comparison along the upper edge of the beam.

In the first case, the upper edge is in compression in the y direction, so the graph shows negative strains. There is a slight assymetricality to the results which may be attributed to the supports and numerical errors in the solution.

In the middle section, all the solutions seems to converge to the same amount of compression except for the Q4 element, which for the first two mesh configurations (6x1 and 12x6 elements), shows lower values along the length of the beam. Possible reason is the relatively small number of elements in the x direction.

In the parts above supports, the otained values diverge, however, the strains obtained with PS element from σ field show the highest strains, with the Q4 element steadily obtaining strains lower strains. The strain obtained with PS element from u field show values approximately in the middle of the two.

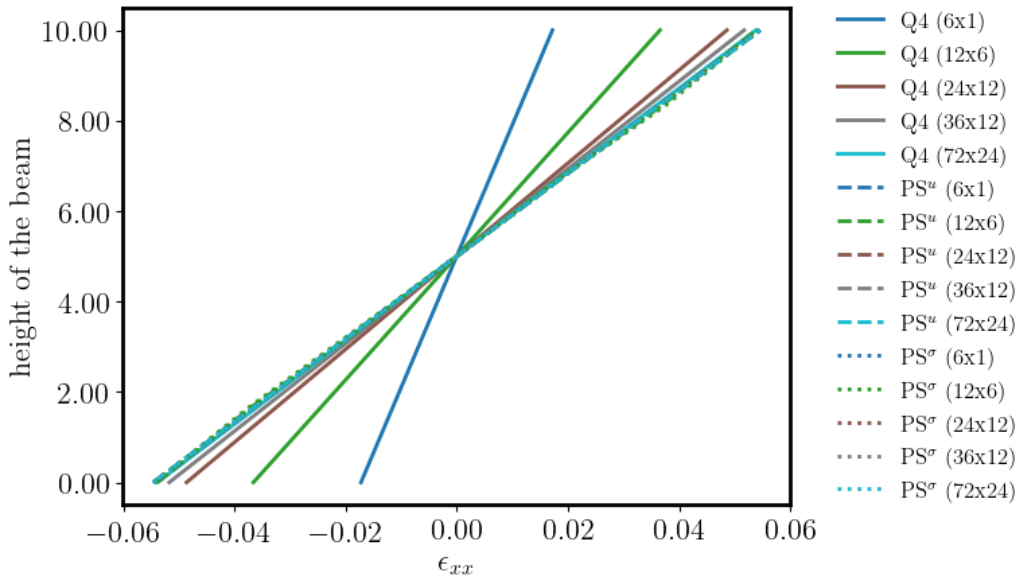

Figure 6.8: ε_{xx} comparison along the middle section of the beam.

The second graph shows the strains in x direction along the middle section. The values of this particular section are crucial for design of beams in bending.

As expected the upper part of the section is subjected to tension while the lower part is subjectedd to compression. Given that the beam is loaded by bending moment, neutral axis goes through the middle of the section.

As in the previous case, the worst results were obtained by the coarsest mesh of the Q4 elements. Finer mesh of the same element subsequently converges to the values obtained by the PS element. For the strains obtained by the PS element (both fields) the solution differ only marginally. The solutions are similar both for the same mesh configuration and different fields strain, and for the different mesh density of the same field strains. Interestingly enough, the first similarity is in direct opposition to the element behaviour observed in the previous case, where strains obtained by the two field differed considerably.

The latter only confirms the convergence analysis, which showed excellent results by the PS element when only minimum number of elements is present.

6.3 Cook's membrane: nearly incompressible material

Cook's membrane is one of the common examples to test element's performance on a nearly incompressible material [47, 48]. It consists of a tapered panel of nearly incompressible material clamped at one side, loaded by traction (see Figure 6.9 further on). Response of the structure combines shear and bending.

Two types of the analysis may be found in literature: (a) non-linear analysis using finite deformations with incompressible or nearly incompressible material [48, 47]), or b) linear elastic analysis with nearly incompressible material, [49, 50, 6].

The second example will be done in the framework of the thesis. Based on the analysis done by César de Sá & Natal [6], two cases of nearly incompressible material will be tested: (i) $\nu = 0.4999$, (ii) $\nu = 0.4999999$. Modulus of elasticity for both equals to $E = 240.565$. Full quadrature is used. See the geometry in consistent system of units in Figure 6.9).

The aim of the study is to analyze convergence of results for both elements with increasing mesh density (elements per side) and subsequently compare the results with those obtained by César de Sá & Natal. In their analysis, they offer results for the following elements:

- Qi5: element with two extra compatible deformation modes,
- Qi6: element inspired by Qi5 element where "an extra field of variables related to the space derivatives of the displacement field is added",
- SRI: element with selective reduced integration on the volumetric terms, where the deviatoric part of the stifness matrix is fully integrated,
- QM6: incompatible modes element, equivalent to the element by Simo and Rafai [33],
- **B**-bar method element which "avoides the necessity of reduced integration and in which the shape function derivatives related to the volumetric response were replaced by approximations resulting from a mixed formulation".

Six mesh configurations are tested: (a) 1 element, (b) 2 elements per side, (c) 4 elements per side, (d) 8 elements per side, (e) 16 elements per side, (f) 32 elements per side. Vertical displacement in point $A[48, 60]$ is compared.

Figure 6.11 shows result obtained for the nearly incompressible material of $\nu = 0.4999$. From the results obtained by César de Sá and Natal, all elements apparently converge to the same solution. The Pian-Sumihara element shows convergence to the same result. However, when there are only few elements on the side of the membrane (approximately <5),

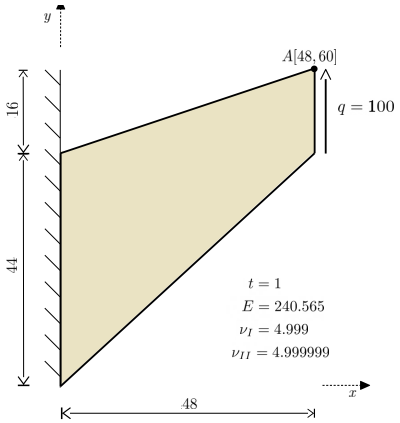

Figure 6.9: Cook's membrane geometry and material properties [6].

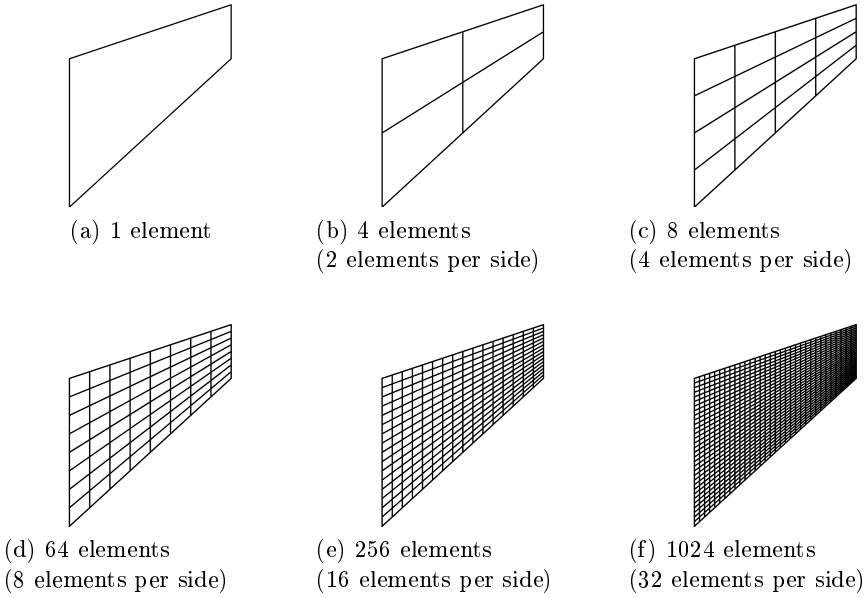

Figure 6.10: Mesh configurations of Cook's problem.

the Pian-Sumihara element shows slightly better results than most of the other elements, with the exception of the Qi6 element developed specifically for nearly incompressible material [6]. The Q4 shows poor quality of results, however, certain improvement is detectable as the number of elements per side rises. Nevertheless, the element still doesn't converge to the same solution as the other elements.

In the case of the second material (Figure 6.12), which is closer to the incompressibility limit with $\nu = 0.4999999$, the Pian-Sumihara element also shows high quality results even when compared to the other elements. Repeating the behaviour as in the case of the previous material, the element shows especially good results when the membrane is discretized into fewer elements. Only the QM6 element shows slightly better results. As in the pre-

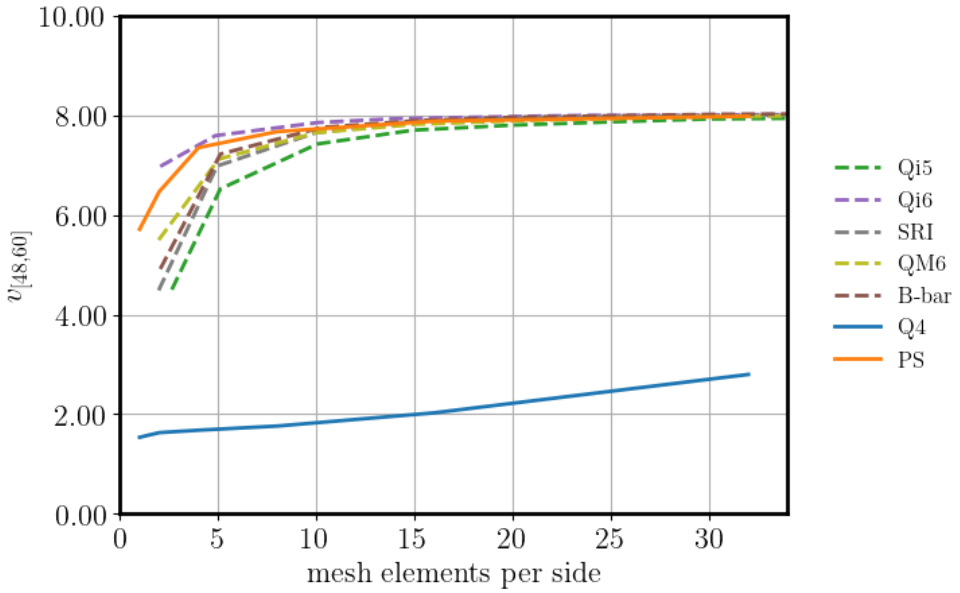

Figure 6.11: Graph of the convergence analysis results for $\nu = 0.4999$, dashed line results were obtained from [6].

vious case, all the elements with the exception of the Q4 material converge to the same solution.

The Q4 element results do not improve as more elements are added, suggesting that volumetric locking is present and the element is not able to capture the membrane's deformation due to the near incompressibility of the material.

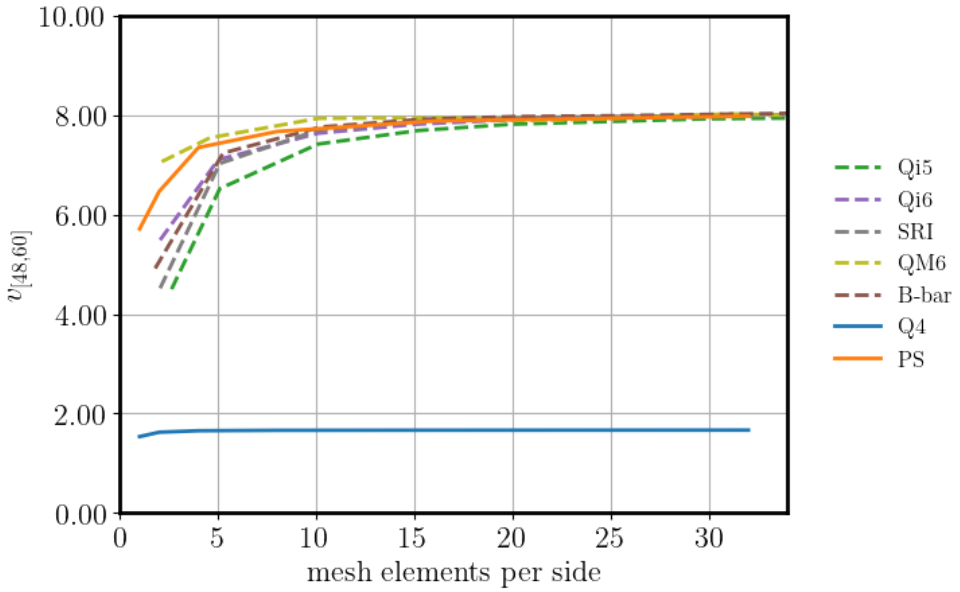

Figure 6.12: Graph of the convergence analysis results for $\nu = 0.4999999$.

6.4 Locking problem

In the last analysis, the elements are tested for locking in distortion based on an analysis done by César de Sá & Natal in [6]. The basic geometry of the problem is displayed in Figure 6.13. It consists of a 2x2 mesh and three loads. Horizontal displacements of nodes 1, 7 and 9 are compared. Full integration is used.

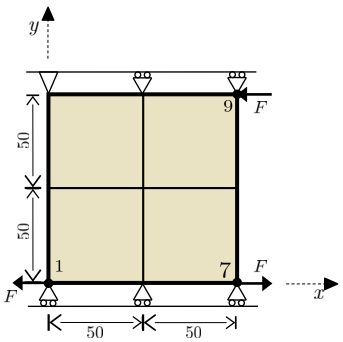

Figure 6.13: Non-distorted basic geometry of the test case described in [6].

Two types of distortions are tested with nearly incompressible material:

- displaced middle node,
- rotated inner elements edges.

The following paragraphs describe each case to more detail and show results.

Nearly incompressible material analysis with distorted mesh is done on the following four cases with specific distortion with full integration implemented.

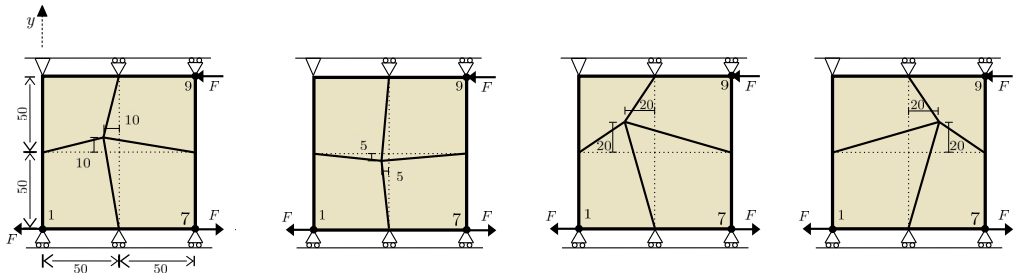

Figure 6.14: Nearly incompressible material test cases with middle node distortion.

Each mesh is tested with rising ratio of Lamé's parameters λ and μ [10]. It transforms to the Poisson's coefficient in the following manner:

$$\frac{\lambda}{\mu} = \frac{\nu}{2(1-2\nu)} \tag{6.1}$$

In the analysis the term $\log(\lambda/\mu)$ ranges from 1 to 15, where 1 corresponds to $\nu = 0.4878$ and 15 limitly approaches to the incompressibility limit of $\nu = 0.5$.

The first part compares the displacement of nodes 1 and 9 as the material approaches to incompressibility and compares the distorted solution to the one obtain with regular mesh. The first graph (Figure 6.15) shows displacements of nodes 1 and 9 for both elements in the absolute values of the displacement. The absolute values are largely similar, as the structure is loaded symmetricaly. As the Poisson's coefficient rises, the Q4 element locks and the values converge to zero, not giving any result. The PS element gives high quality results until approximately $\log(\lambda/\mu) = 13$, then it is no longer able to capture the deformation. There is a slight rise in the values at the beginning which can be attributed to the rising Poisson's coefficient. The change is not noticeable further on because the value of ν limitly approaches to 0.5.

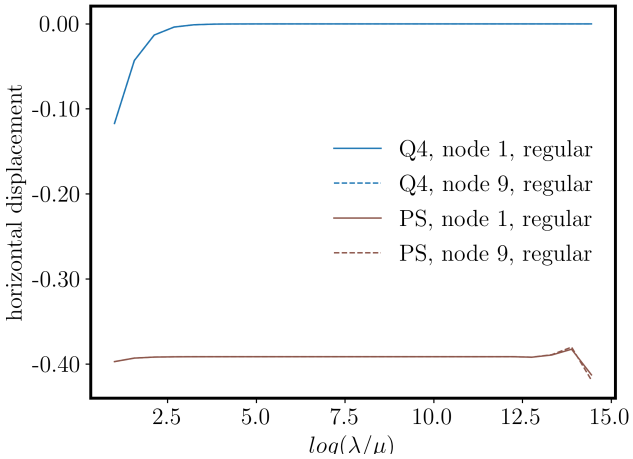

Figure 6.15: Resulting displacement of nodes 1 and 9 as obtained by regular mesh.

Figures Figures 6.14a to 6.14d than show the difference between the results obtained by a regular mesh and the distorted mesh.

As in the case of previous mesh, in all four cases the Q4 element locks and gives zero displacements. The PS element error corresponds to the amount of distortion, confirming the results obtained in section 6.1. The results are also dependent on the direction in which the central node was distorted in relation to the observed nodes. Nevertheless, the error of the PS element is not influenced by rise of the Poisson's coefficient until approximately $\log(\lambda/\mu) = 12.5$ in all four cases.

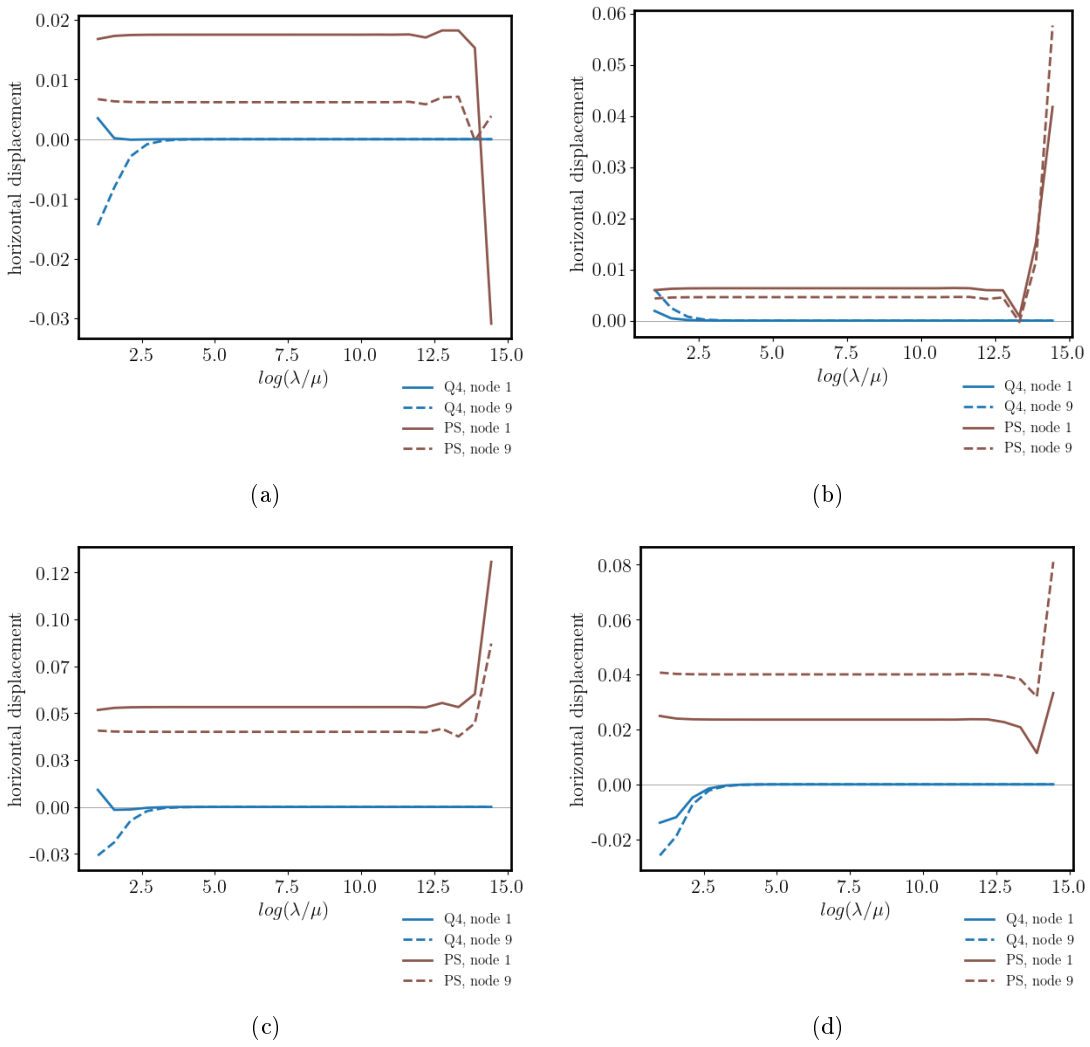

Figure 6.16: Error in displacement of nodes 1 and 9 when mesh is distorted.

In the final analysis the near incompressible material is tested in combination with inner mesh edges rotation as on the following Figure. The mesh is rotated by angle $\alpha \in \langle -45°, 45° \rangle$, while the incompressibility is kept at $\log(\lambda/\mu) = 9$.

Displacement of nodes 1 and 7 is observed. In non-distorded mesh, $v_1 = -0.395$ while $v_7 = 0$. Figure 6.18 shows obtained displacements for both nodes depending on the rotation angle.

Interestingly enough, the results show similar response by both elements to rotation in both directions resulting in symmetrical graph. The displacement of node number seven in regular and rotated mesh does not differ. It is equal to zero for both types of elements. In case of node 1, the displacement response to mesh rotation differs between the two elements.

In case of the Q4 element, it appears to become less stiff with increasing rotation of mesh, which results in higher displacements of the node. With increasing rotation,

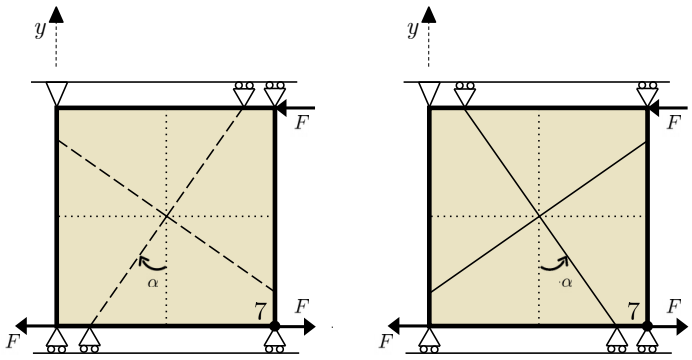

(a) (b)

Figure 6.17: Nearly incompressible material test case with inner element edges rotation around the central node.

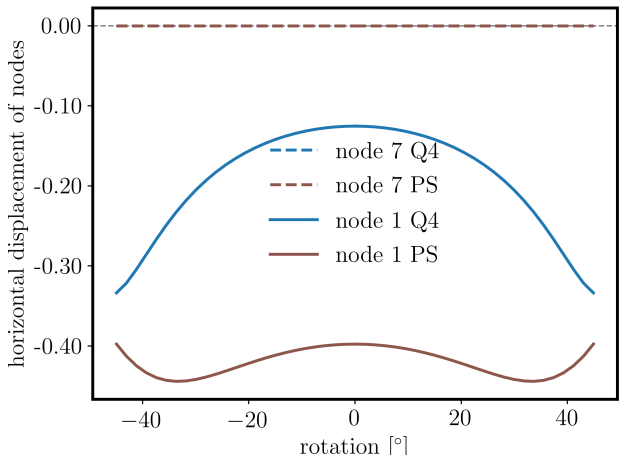

Figure 6.18: Displacements of nodes 1 and 7 depending on mesh rotation.

the element offers better results, however, the results are underestimated in comparison to the results offered by the PS element.

In case of the Pian-Sumihara element, the obtained displacement slightly rises until about 35° of rotation in both clockwise and anticlockwise direction. After passing the 35° rotation, the displacement steeply falls back to the value obtained by regular mesh. In either case, no locking is apparent.

Chapter 7

Conclusion

Linear elasticity idealization of behavior of structures is a crucial stepping stone in approximating the behavior of solid parts or structures of various scales. However in order to acquire quality results based on which it is possible to design a structure, it is necessary to understand the context of the idealization and the method which is applied to obtain results.

In light of the above written, the thesis aimed to provide both. To describe both the idealization of a linearly deforming solid body in a static regime and to describe one of the most widely used method of today to solve the equations, the Finite Element Method. One of the simple popular elements has been described along with an alternative of mixed-field formulation to account for possible shortcomings of the first formulation, with both being implemented, validated and tested against well-known benchmark problems of literature.

In the first part, theoretical background to linear elasticity in strong form and subsequently the derivation of equivalent variational weak forms as a possible basis to the formulation of the Finite Element Method have been provided.

The second part described a general way of deriving the FEM as part of the weighted residual methods in the beginning, followed by additional approaches and techniques which are commonly used in the software implementation of the method. That is the concept of shape functions, essential to the method as they create the elements. Subsequently, the description of numerical integration via Gauss quadrature was described along with the concept of isoparametric elements, which allows convenient use of the numerical integration to evaluate integrals in a local, natural coordinate system.

The theoretical part was followed by description of two specific elements in the context of software implementation, which included specific ways of building matrices of shape functions and their derivatives.

The first implemented element is the plane stress/strain quadrilateral bilinear isoparametric element, called the Q4 element in literature. The element is based on the irreducible, displacement-based variational principle described in the first section. It is one of the simplest formulation, as only displacement field is obtained in the computation, with strain

and stress field derived based on displacements.

The second implemented element is based on the Hellinger-Reissner variational principle. Two primary fields are approximated independently, displacements and stresses. While unknown parameters to the displacement field are nodal displacements, normal stresses in both directions are approximated with linear and constant components and shear stress is approximated by constant component only. The element was described as developed by Pian & Sumihara in [5].

Subsequent section describes situations in which an element shows higher stiffness and thus endangers the outcome of the design process by providing wrong results on the dangerous side. This behavior, known as locking, is especially related to the bilinear Q4 element, which in bending dominated situations and in case of near incompressible material shows either stiffer behavior of zero displacements.

Last teoretical chapter describes requirements to Finite Element Method formulations to deliver adequate results in application and provides different tests the validate an implementation.

Following the theoretical description, a Finite Element Method algorithm was developed with the two mentioned elements implemented, to be later applied in border-line situations where the Q4 element tends to lock and/or in distortion which may influence element performance. To apply the algorithm, a validation has been done by patch test and comparison to results of four bending dominated cases from literature was done.

The first in the series of benchmark cases to test and compare both elements was an analysis of distortion effect on structure consisting of two elements. Both types of elements showed best results in non-distorted form, however, the Pian-Sumihara element show about 40% better results, whatever distortion is applied.

Next, a deformation of a beam in bending was obtained by both elements. A h-refinement was performed and convergence observed. In the analysis, the Pian-Sumihara element provided near exact solution to the problem with only minimum elements present, while the locking in Q4 element had to be compensated by computationally demanding high number of elements for the solution to converge. Normal strains by the upper edge and along middle vertical section were also compared to observe their dependency on the primary field from which they were derived.

In the subsequent problem, bending dominated behavior with shear combined with nearly incompressible material has been modeled in a classic problem, the Cook's membrane. Convergence rate was tested and compared to other elements from literature which also aimed to solve the locking problem and were tested against this particular problem. As in the previous cases, performance of the Q4 element has been inferior to all other elements as it was showing locking. However, the Pian-Sumihara element showed comparable behavior to the other elements, regarding the convergence rate.

The final analysis considered the distortion effect on a nearly incompressible material. Firstly the elements were tested as the Poisson's coefficient approaches the incompresibility

limit. While the Pian-Sumihara element showed solid results, the Q4 element exhibited locking early on. Subsequently, the elements were distorted and the difference to the results obtained with regular mesh has been observed. While the Q4 element exhibited locking, the Pian-Sumihara element showed error related to the amount of disturbence to the regular mesh.

7.1 Limitations

Although linear elastostatics is widely used, one of the assumptions is that only small deformations with regard to the overall dimensions of the structure occur. Neither the theoretical part of the thesis nor the subsequent analysis of elements behavior adresses large deformations, limiting the scope of the thesis and also the interpretation of results. Similarly, elastic behavior is only applicable to certain materials, which restricts the applicability of results.

The results were obtained presuming static behavior of applied forces and their effects, not considering possible dynamic effects.

Last but not least, possible remedies for shear and volumetric locking were briefly described and one analysis was done considering alternative methods to the mixed-field formulation as remedies, however, the comparison of two element formulations is not sufficient to evaluate the element's efficiency in context of other methods.

7.2 Future work

With regard to the limitations of the results following future research is proposed:

- Compare the Pian-Sumihara element to other elements developed specifically to account for locking behavior.
- Implement non-linear model of a plastic deformation based on the Hellinger-Reissner principle.
- Extend the scope of the algorithm to finite deformations.

References

[1] O. C. Zienkiewicz, R. L. Taylor, and J. Zhu, *The Finite Element Method: Its Basis and Fundamentals*, 2013.

[2] M. Radi, "Three-Dimensional Simulation of Thermal Oxidation," Ph.D. dissertation, 1998. [Online]. Available: https://www.iue.tuwien.ac.at/phd/radi/diss.html

[3] E. Wilson, R. Taylor, W. Doherty, and J. Ghaboussi, *Incompatible Displacement Models*. ACADEMIC PRESS, INC., 1973. [Online]. Available: http://dx.doi.org/10.1016/B978-0-12-253250-4.50008-7

[4] C. A. Felippa, "Introduction to Finite Element Methods," 2004.

[5] T. H. H. Pian and K. Sumihara, "Rational approach for assumed stress finite elements," *International Journal for Numerical Methods in Engineering*, vol. 20, no. 9, pp. 1685–1695, sep 1984. [Online]. Available: http://doi.wiley.com/10.1002/nme.1620200911

[6] J. M. César De Sá and R. M. Natal Jorge, "New enhanced strain elements for incompressible problems," *International Journal for Numerical Methods in Engineering*, vol. 44, no. 2, pp. 229–248, 1999.

[7] A. F. Bower, *Applied mechanics of solids*, 2010.

[8] E. Tonti, *The Mathematical Structure of Classical and Relativistic Physics: A General Classification Diagram*. Springer New York, 2013.

[9] K. Washizu, *Variational Methods in Elasticity & Plasticity*, 1968.

[10] O. Zienkiewicz, R. Taylor, and D. Fox, *The Finite Element Method for Solid and Structural Mechanics*, 6th ed. Elsevier Butterworth-Heinemann, 2014.

[11] J. Fish and T. Belytschko, *A first course in finite elements*, 2008, vol. 45, no. 06.

[12] M. Tchonkova and S. Sture, "Classical and Recent Formulations for Linear Elasticity," *Archives of Computational Methods in Engineering*, vol. 8, no. 1, pp. 41–74, 2001.

[13] C. Lanczos, "The Variational Principles of Mechanics," p. 464, 1952.

[14] M. Smith, *ABAQUS/Standard User's Manual, Version 6.9*. United States: Dassault Systèmes Simulia Corp, 2009.

[15] O. C. Zienkiewicz, "Displacement and equilibrium models in the finite element method by B. Fraeijs de Veubeke, Chapter 9, Pages 145–197 of Stress Analysis, Edited by O. C. Zienkiewicz and G. S. Holister, Published by John Wiley & Sons, 1965," *International Journal for Numerical Methods in Engineering*, vol. 52, no. 3, pp. 287–342, 2001.

[16] O. C. Zienkiewicz, R. L. Taylor, and P. Nithiarasu, *The Finite Element Method for Fluid Dynamics: Seventh Edition*, 2013.

[17] J. M. César De Sá, "Métodos de Aproximação em Engenharia."

[18] R. C. Wylie and L. C. Barrett, *Advanced engineering mathematics*. McGraw-Hill, 1986. [Online]. Available: https://books.google.cz/books?id=Ob0owQEACAAJ

[19] J. L. Krahula and J. F. Polhemus, "Use of fourier series in the finite element method," *AIAA Journal*, vol. 6, no. 4, pp. 726–728, 1968.

[20] I. Babuška, "The p and h-p Versions of the Finite Element Method: The State of the Art," pp. 199–239, 1988.

[21] K. J. Bathe, *Finite Element Procedures*, 1996. [Online]. Available: http://www.amazon.com/Finite-Element-Procedures-Part-1-2/dp/0133014584

[22] G. Sineri, "Finite Element Formulations for Isotropic and Anisotropic Materials: a comparison between different approaches," 2015.

[23] H. Gavin, "Mathematical Properties of Stiffness Matrices," *Matrix Structural Analysis*, vol. 2, no. 3, pp. 1–6, 2006.

[24] R. Piltner, "An alternative version of the Pian-Sumihara element with a simple extension to non-linear problems," *Computational Mechanics*, vol. 26, no. 5, pp. 483–489, 2000.

[25] R. J. Guyan, "Reduction of stiffness and mass matrices," *AIAA Journal*, vol. 3, no. 2, p. 380, 1965.

[26] J. M. De César Sá, R. M. Natal Jorge, R. A. Fontes Valente, and P. M. Almeida Areias, "Development of shear locking-free shell elements using an enhanced assumed strain formulation," *International Journal for Numerical Methods in Engineering*, vol. 53, no. 7, pp. 1721–1750, 2002.

[27] L. Yunhua, "Explanation and elimination of shear locking and membrane locking with field consistence approach," *Computer Methods in Applied Mechanics and Engineering*, vol. 162, no. 1-4, pp. 249–269, 1998.

[28] Y.-H. Luo, "On shear locking in finite elements," Ph.D. dissertation, 1997.

[29] R. J. Alves De Sousa, R. M. Natal Jorge, R. A. Fontes Valente, and J. M. César De Sá, *A new volumetric and shear locking-free 3D enhanced strain element*, 2003, vol. 20, no. 7-8.

[30] I. Babuška and M. Suri, "On Locking and Robustness in the Finite Element Method," *SIAM Journal on Numerical Analysis*, vol. 29, no. 5, pp. 1261–1293, 1992.

[31] F. Auricchio, L. Beirão Da Veiga, C. Lovadina, and A. Reali, "Enhanced strain methods for elasticity problems," *ECCOMAS 2004 - European Congress on Computational Methods in Applied Sciences and Engineering*, pp. 1–16, 2004.

[32] R. Piltner and R. L. Taylor, "A quadrilateral mixed finite element with two enhanced strain modes," *International Journal for Numerical Methods in Engineering*, vol. 38, no. 11, pp. 1783–1808, 1995.

[33] J. C. Simo and M. S. Rifai, "A class of mixed assumed strain methods and the method of incompatible modes," *International Journal for Numerical Methods in Engineering*, vol. 29, no. 8, pp. 1595–1638, 1990.

[34] J. A. Baier-Saip, P. A. Baier, A. R. de Faria, J. C. Oliveira, and H. Baier, "[notes] Shear locking in one-dimensional finite element methods," *European Journal of Mechanics, A/Solids*, vol. 79, no. October 2019, p. 103871, 2020. [Online]. Available: https://doi.org/10.1016/j.euromechsol.2019.103871

[35] R. L. Taylor, J. C. Simo, O. C. Zienkiewicz, and A. C. Chan, "The patch test—a condition for assessing FEM convergence," *International Journal for Numerical Methods in Engineering*, vol. 22, no. 1, pp. 39–62, 1986.

[36] K.-J. Urgen Bathe, "The inf±sup condition and its evaluation for mixed finite element methods," *Computers and Structures*, vol. 79, no. 79, pp. 243–252, 2001.

[37] G. P. Bazeley, Y. K. Cheung, B. M. Irons, and O. C. Zienkiewicz, "Triangular elements in plate bending - conforming and non-conforming solutions," pp. 547–576, 1966.

[38] I. Babuška and R. Narasimhan, "The Babuška-Brezzi condition and the patch test: An example," *Computer Methods in Applied Mechanics and Engineering*, vol. 140, no. 1-2, pp. 183–199, 1997.

[39] F. Brezzi, "On the existence, uniqueness and approximation ofsaddle-point problems arising from lagrangian multipliers," *Recherche*, 1974.

[40] I. Babuška, "The finite element method with Lagrangian multipliers," *Numerische Mathematik*, vol. 20, no. 3, pp. 179–192, 1973.

[41] O. C. Zienkiewicz, S. Qu, R. L. Taylor, and S. Nakazawa, "The patch test for mixed formulations," *International Journal for Numerical Methods in Engineering*, vol. 23, no. 10, pp. 1873–1883, 1986.

[42] G. Van Rossum and F. L. Drake, *Python 3 Reference Manual*. Scotts Valley, CA: CreateSpace, 2009.

[43] T. Oliphant, "{NumPy}: A guide to {NumPy}," USA: Trelgol Publishing. [Online]. Available: http://www.numpy.org/

[44] J. D. Hunter, "Matplotlib: A 2D graphics environment," *Computing in Science & Engineering*, vol. 9, no. 3, pp. 90–95, 2007.

[45] C. U. Nguyen and A. Ibrahimbegovic, "Hybrid-stress triangular finite element with enhanced performance for statics and dynamics," *Computer Methods in Applied Mechanics and Engineering*, vol. 372, p. 113381, 2020. [Online]. Available: https://doi.org/10.1016/j.cma.2020.113381

[46] P. Wriggers and J. Korelc, "On enhanced strain methods for small and finite deformations of solids," *Computational Mechanics*, vol. 18, no. 6, pp. 413–428, 1996.

[47] U. Brink and E. Stein, "On some mixed finite element methods for incompressible and nearly incompressible finite elasticity," *Computational Mechanics*, vol. 19, no. 1, pp. 105–119, 1996.

[48] J. C. Simo and F. Armero, "Geometrically non-linear enhanced strain mixed methods and the method of incompatible modes," *International Journal for Numerical Methods in Engineering*, vol. 33, no. 7, pp. 1413–1449, 1992.

[49] "Swansea University Prifysgol Abertawe Mixed Galerkin And Least-Squares Formulations For Isogeometric Analysis," 2014.

[50] K. B. Nakshatrala, A. Masud, and K. D. Hjelmstad, "On finite element formulations for nearly incompressible linear elasticity," *Computational Mechanics*, vol. 41, no. 4, pp. 547–561, 2008.